Review Article

ADVANCED IMAGING

Review of polarimetric image denoising

Hedong Liu,[a] Xiaobo Li,[a] Zihan Wang,[b] Yizhao Huang,[b] Jingsheng Zhai,[a] and Haofeng Hu[a,b,*]

[a]School of Marine Science and Technology, Tianjin University, Tianjin, China

[b]School of Precision Instrument and Opto-electronics Engineering, Key Laboratory of Opto-electronics Information Technology, Ministry of Education, Tianjin University, Tianjin, China

Abstract. Polarimetric imaging, leveraging measurements of polarimetric parameters that encode distinct physical properties, finds wide applications across diverse domains. However, some critical polarization information is highly sensitive to noise, and denoising polarimetric images while preserving polarization information remains a challenge. The development of denoising techniques for polarized images can be roughly divided into three stages: The first stage involves the direct application of traditional image denoising algorithms, such as spatial/transform domain filtering. The second stage involves specially designed methods for polarized images, using image prior models for noise removal, such as principal component analysis and K-singular value decomposition. In the third stage, benefiting from advances in deep learning, denoising methods tend to integrate polarization characteristics with deep learning models for noise suppression. The residual dense network, U-Net, and other effective models are appropriately modified and supervised/self-supervised trained to handle the denoising problem of regular/extensive polarimetric images. In this paper, we perform a comparative study of polarimetric image denoising methods. These methods are first classified as learning-based and traditional methods. Then, the motivations and principles of different types of denoising methods are analyzed. Finally, some potential challenges and directions for future research are pointed out.

Keywords: polarimetric imaging; image denoising; deep learning; noise model; convolutional neural network.

Received Apr. 15, 2024; revised manuscript received Jul. 19, 2024; accepted Sep. 4, 2024; published online Oct. 10, 2024.

[DOI: 10.3788/AI.2024.20001]

1. Introduction

Image degradation caused by noise is a typical issue for applications of various optical imaging. Therefore, image denoising holds significant importance in optical imaging systems, garnering widespread interest across academia and industry. Conceptually, image denoising can be viewed as a specialized instance within the realm of inverse problems, wherein the objective is to restore the information within noisy observations[1]. In real-world applications, it functions as a preliminary stage preceding various subsequent tasks, including classification[2], detection[3], and segmentation[4].

Recently, advances in imaging and optical technologies have greatly enriched the physical information captured and persevered by multiple sources and dimensions of images. The enhancements allow for a richer representation and more accurate depiction of real-world scenes[5–7]. For instance, polarization describes the direction of vibration of the photoelectric field. Based on the measurement and processing of polarization information, polarimetric imaging can capture the characteristics of object shape, surface roughness, and texture. Thus, it has been applied in material classification[8,9], image dehazing[10–12], 3D shape reconstruction[13,14], target detection[15,16], and biomedical imaging[17,18]. Furthermore, advancements in polarization camera technology enable the capture of multiple polarized images of a scene simultaneously, each with varying polarization angles[19–21], which enhances the feasibility of employing polarimetric imaging in the aforementioned applications. However, the introduction of polarization also posts greater demands and challenges on denoising, especially in photon-starved conditions, for instance, employing ultrafast imaging with a high frame rate or taking a photo under low-light conditions[22,23].

First, some crucial polarization information, such as the angle of polarization (AoP) and degree of polarization (DoP), are

*Address all correspondence to Haofeng Hu, haofeng_hu@tju.edu.cn

nonlinear combinations of Stokes parameters. Nonlinear operators can amplify the influence of noise. Therefore, they are very sensitive to noise. Moreover, the polarizer, which is essential for obtaining polarimetric images, will attenuate beam intensity, leading to a diminished signal-to-noise ratio (SNR). Therefore, polarimetric images are noisy and can be detrimental to subsequent polarization analysis and applications. Second, another challenge in polarimetric image processing involves efficiently leveraging the interrelated physical information across polarization channels[24–26], while simultaneously achieving a harmonious equilibrium between noise reduction and polarization information preservation. Because the implicit physical correlation in the polarization dimension is excessively complex, effectively exploiting the correlation between dimensions and restoring precise physical information from noisy polarimetric images remains a challenge. Hence, there is significance in developing denoising algorithms specifically tailored for polarimetric images.

Conventional denoising techniques elaborate models and priors based on total variation (TV)[27], sparse representation[28], non-local self-similarity[29], and so on. Among these methods, block-matching and 3D filtering (BM3D), introduced by Dabov *et al.*[30], stands out as one of the most remarkable denoising techniques. BM3D uses the self-similarity of natural images by operating non-locally similar block matching then collaborative filtering in the 3D transform domain. Polarimetric imaging benefits from improved denoising methods[31], and some denoising methods can be extended and applied to the polarization domain. For example, by applying a certain decorrelation transform[32] or modeling the channel correlation[33], the prominent BM3D approach has also found successful adaptation for polarimetric image denoising.

Due to their flexibility and modeling ability, methods relying on deep neural networks (DNNs) have garnered remarkable achievements in the domain of image denoising[47]. In contrast to conventional denoising techniques that solely rely on internal information derived from noisy observations, deep-learning-based methods typically employ supervised training strategies, where large-scale datasets guide the process to minimize the error between the target and prediction. Recently, convolutional neural networks (CNNs) have emerged as promising methods for image denoising[48–50], leading to substantial advancements in denoising performance. The applicability of CNNs extends beyond traditional image denoising, as they have also demonstrated remarkable effectiveness in processing noisy polarimetric images[51–53]. However, applying conventional image denoising techniques directly to images captured by imagery polarimeters may not be practical, primarily due to the inherent physical characteristics of polarization images. Improvements to the CNN are needed to adopt CNN for polarimetric images. Moreover, collecting a substantial amount of accurately labeled high-quality polarimetric images is a time-consuming task. Consequently, alternative research approaches have aimed to mitigate the necessity for extensive noisy-clean datasets[54,55].

The objective of this review is to offer a comprehensive overview for diverse methods that have advanced the domain of polarimetric image denoising. An outline of this survey is shown in Fig. 1(a), and we summarize various polarimetric image denoising methods into a tree diagram in Fig. 1(b). Various methods in recent years have been classified into traditional methods and DNN-based methods, with a chronological arrangement along a timeline. In this review, Section 2 describes the model of noise and analyzes the influence of noise in polarimetric imaging. Section 3 provides a brief review of generic image denoising methods related to polarimetric image denoising. Section 4 provides a review of traditional approaches to polarimetric image denoising. Section 5 presents an extensive literature survey concentrating on learning-based denoising methods designed for

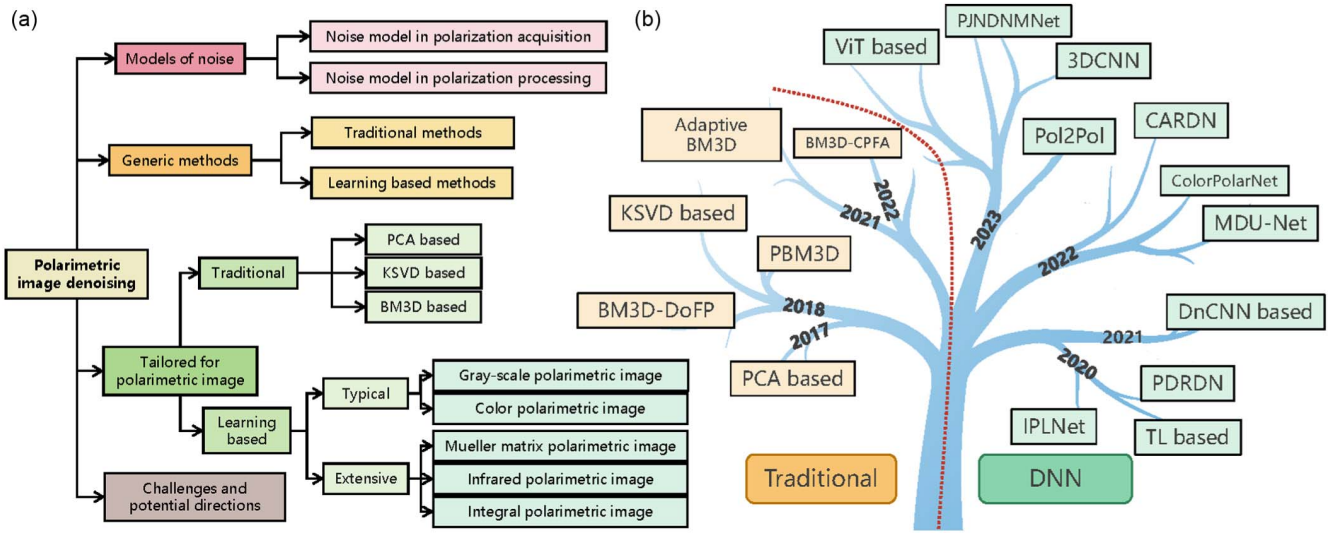

Fig. 1 The whole framework figure. (a) Outline of the review. It consists of four parts, including noise models, generic methods, denoising methods tailored for polarimetric images, and challenges and potential directions. (b) Timeline and classification of polarimetric image denoising works in recent years, including PCA-based[34], BM3D-DoFP[35], PBM3D[32], KSVD-based[36], Adaptive BM3D[37], BM3D-CPFA[33], IPLNet[38], TL-based, PDRDN[39], DnCNN-based[40], MDU-Net[41], ColorPolorNet[42], CARDN[43], 3DCNN[44], PJNDNMNet[45], Pol2Pol[116], and ViT-based[46] methods.

various types of polarimetric images. In Sec. 6, we discuss the challenges and potential directions. In Sec. 7, we summarize this review and provide a conclusion.

2. Model of Noise in Polarimetric Imaging

First, the source of noise for polarimetric imaging is analyzed, and then we describe how noise characteristics are changed with each step in the imaging pipeline. Next, we assess the average error rates associated with polarization-related parameters. Our analysis reveals that measurements of DoP and AoP are highly susceptible to noise, with even minor levels of noise causing significant deviations in measured values. Hence, there is significant interest in improving polarimetric image quality to ensure accurate acquisition of DoP and AoP.

2.1. Noise Model in Polarization Acquisition

The denoising process tends to be issue-specific and depends upon the type of image and noise model[56,57]. A common approximation of the image noise model can be stated as

$$\mathbf{I}^n(x,y) = \mathbb{W}\mathbf{S}(x,y) + \mathbf{N}(x,y), \tag{1}$$

where $\mathbf{I}^n(x,y)$ means a noisy polarimetric image at position (x,y), $\mathbb{W}$ denotes the measurement matrix depending on the eigenstate of polarization state analysis in the polarimetric imaging system, $\mathbf{S}(x,y) = [S_0(x,y), S_1(x,y), S_2(x,y), S_3(x,y)]^{\mathrm{T}}$ represents the clean image of the Stokes vector, and $\mathbf{N}(x,y)$ refers to a noise component of observation[58].

In practice, the noise component may be caused by various intrinsic (sensors, image capture devices, etc.) and extrinsic factors that are often not feasible to escape in practical circumstances. In this section, as depicted in Fig. 2, we adopt the physics-based noise formation model, which is based on the intrinsic pipeline of optical imaging and considers the process of photons through multiple stages. This model intricately represents sensor noise, encompassing multiple noise sources. Letting N_p be photon shot noise, N_{read} be readout noise, N_b be banding pattern noise, and N_q be quantization noise, the noise model of polarimetric imaging[59,60] can be expressed as

$$N = KN_p + N_{\text{read}} + N_b + N_q, \tag{2}$$

where K is the gain of the imaging system.

When light interacts with the pixel area of the photosensor, the number of electrons generated has uncertainty, which is proportional to the incident light intensity. Noise arises due to the probabilistic nature of light, known as photon shot noise. This noise follows a Poisson distribution and is inherent to all sensors, even in an ideal scenario, representing a fundamental constraint.

During the conversion of electrons into voltage, a series of processes including integration, amplification, and readout occur, resulting in measurable charge or voltage at the end of the capturing period. In this electron-to-voltage conversion phase, pixel circuit noise is introduced, and it varies based on circuit design and processing technology. This noise includes dark current noise, thermal noise, and source follower noise. Additionally, band pattern noise denoted as N_b appears as regular striped patterns in images and is typically modeled as a zero-mean Gaussian distribution. For simplicity, we combine multiple noise sources into a unified parameter termed read noise N_{read}, often approximated by a Gaussian distribution or, more precisely, a Tukey lambda distribution.

When the readout analog voltage signal is converted into a digital signal using an analog-to-digital converter (ADC), the finite precision will introduce quantization noise N_q. Assuming q is the quantization step, quantization noise is typically assumed to follow a uniform distribution $U(-1/2q, 1/2q)$.

Other sources of noise are also introduced during the capture process, such as dark current noise, reported by a lot of previous literature[61,62]. They have minimal contribution to imaging results. Therefore, for simplicity, other noises will be ignored in this analysis. In addition, although external factors can also affect image noise, the complexity, unpredictability, and limited

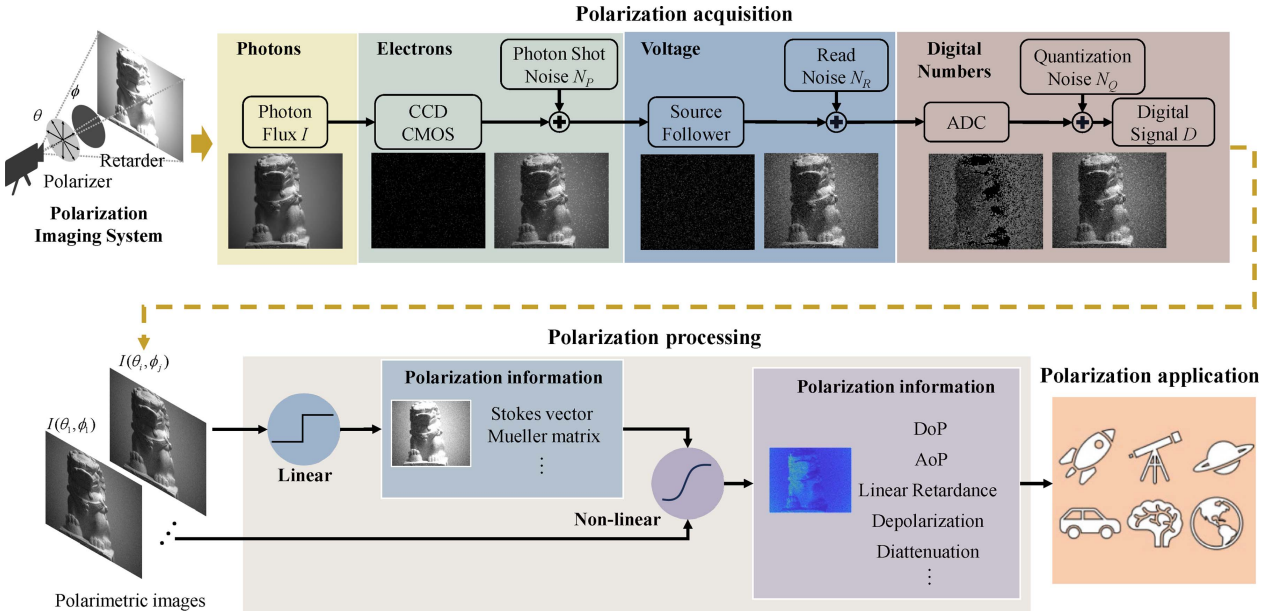

Fig. 2 The diagram of the noise formation model.

control over these factors make them less prioritized in noise modeling. Therefore, in this section, only internal factors are considered, and the external factors are ignored.

2.2. Noise Model in Polarization Processing

Under ideal conditions without noise, assuming the camera response function is linear, a polarimetric image can be represented as $I(\theta, \phi)$, where θ is the angle of the polarizer and ϕ is the angle of the retarder. When the polarization camera obtains an image, the light may comprise various amplitudes of polarized light. Normally, the following polarimetric images are measured: $\mathbf{I} = [I(0^\circ, 0^\circ), I(45^\circ, 0^\circ), I(90^\circ, 0^\circ), I(135^\circ, 0^\circ), I(45^\circ, 90^\circ)]$. Then, the polarization information can be obtained by linear calculation of these intensity measurements. For example, Stokes vectors are expressed as

$$\mathbf{S} = \begin{bmatrix} S_0 \\ S_1 \\ S_2 \\ S_3 \end{bmatrix} = \begin{bmatrix} I(0^\circ, 0^\circ) + I(90^\circ, 0^\circ) \\ I(0^\circ, 0^\circ) - I(90^\circ, 0^\circ) \\ 2I(45^\circ, 0^\circ) - S_0 \\ 2I(45^\circ, 90^\circ) - S_0 \end{bmatrix}. \tag{3}$$

For simplicity, Eq. (3) is rewritten in the matrix form:

$$\mathbf{I}(x, y) = \mathbb{W}\mathbf{S}(x, y). \tag{4}$$

Since the measurement matrix $\mathbb{W}$ is known for the given polarimetric imaging system, we can obtain the estimator of the Stokes map by inversing the captured noisy image according to Eq. (1); then, we can obtain

$$\hat{\mathbf{S}}(x, y) = \mathbb{W}^+\mathbf{I}^n(x, y) = \mathbb{W}^+[\mathbf{I}(x, y) + \mathbf{N}(x, y)], \tag{5}$$

where "+" denotes the pseudo-inverse of matrix and $\mathbb{W}^+ = (\mathbb{W}^{\mathrm{T}}\mathbb{W})^{-1}\mathbb{W}^{\mathrm{T}}$[63]. We assume that the variance of noise for the jth intensity measurement is equal to σ_j^2. According to Eq. (5), we can calculate the estimation variance of each Stokes parameter as

$$\mathrm{Var}[\hat{\mathrm{S}}(x, y)]_i = \sum_j (\mathbb{W}_{ij}^+)^2\sigma_j^2. \tag{6}$$

These variances indeed depend on the measurement matrix. In addition, it can be seen that the influence of noise is passed from intensity to Stokes parameters through a linear operator. Subsequently, we can obtain images of other polarimetric parameters based on the inverted Stokes maps, such as DoP and AoP:

$$\mathrm{DoP} = \frac{\sqrt{S_1^2 + S_2^2 + S_3^2}}{S_0}, \qquad \mathrm{AoP} = \frac{1}{2} \cdot \arctan\left(\frac{S_2}{S_1}\right). \tag{7}$$

DoP and AoP are nonlinear combinations of these Stokes parameters. Therefore, they are more sensitive to the noise theoretically because the nonlinear operators may amplify the influence of noise. In actual applications, it should be noted that the value of the S_3 component is close to 0. In this case, the DoP in Eq. (7) will be replaced by the degree of linear polarization (DoLP).

To demonstrate the varying sensitivity of polarimetric images, Stokes parameters, DoLP, and AoP to noise, the connections about their mean error rates and noise variance are conducted[64]. The average error rate of a variable x (where x can represent the image of the above polarization information normalized to [0, 1] is defined as

$$\epsilon_x = \sum \left| \frac{\hat{\mathbf{x}} - \mathbf{x}}{\mathbf{x}} \right|. \tag{8}$$

Then, the error rate of S_0 can be derived as

$$\epsilon_{S_0} = \frac{\sum |\hat{S}_0 - S_0|}{\sum S_0} = \frac{\sum \frac{1}{2} |\sum_{i=1}^4 N_i|}{\sum S_0} = \frac{\sum |N_{1,2,3,4}|}{\sum S_0}. \tag{9}$$

Similarly, we obtain the relationship between S_1 and S_2:

$$\epsilon_{S_1} = \frac{\sum |\hat{S}_1 - S_1|}{\sum S_1} = \frac{\sum |N_1 - N_3|}{\sum S_1} = \frac{\sum |N_{1,3}|}{\sum S_1}, \tag{10}$$

$$\epsilon_{S_2} = \frac{\sum |\hat{S}_2 - S_2|}{\sum S_2} = \frac{\sum |N_2 - N_4|}{\sum S_2} = \frac{\sum |N_{2,4}|}{\sum S_2}. \tag{11}$$

Assuming the noise term follows Gaussian distribution and $N_i \sim \mathcal{N}(0, \sigma^2)$, therefore, we can obtain $N_{1,2,3,4} \sim \mathcal{N}(0, \sigma^2)$ and $N_{1,3} = N_{2,4} \sim \mathcal{N}(0, 2\sigma^2)$. Knowing that $\sum S_0 \sum S_1 \approx \sum S_2$ and $\sum |N_{1,2,3,4}| \sum |N_{1,3}| = \sum |N_{2,4}|$, we can derive

$$\epsilon_{S_0}\epsilon_{S_1} \approx \epsilon_{S_2}. \tag{12}$$

Letting p and θ denote the image of DoLP and AoP, the average error rates can be defined as $\epsilon_p = \frac{\sum |\hat{p} - p|}{\sum p}$ and $\epsilon_\theta = \frac{\sum |\hat{\theta} - \theta|}{\sum \theta}$. Due to the complexity of the relationship between error and polarization parameters, it is suspected that DoLP and AoP are more sensitive to noise compared to linear polarization parameters, such as the Stokes vector. To verify this, as shown in Fig. 3, simulations were conducted on 300 synthetic scenes to quantitatively establish the noise sensitivity of the DoLP and AoP. It is evident that, under noisy conditions, there is a significant degradation in the DoLP and AoP, which may result in reduced performance of applications about polarimetric imaging. It is worth noting that the curve of AoP becomes parallel because AoP is very sensitive to noise. The AoP image is completely flooded with noise, so the error reaches saturation. In fact, by visual comparison, AoP images are more sensitive to noise than DoLP images.

3. Generic Image Denoising Methods

Since polarization images share similarities with conventional images at the pixel level, many denoising methods developed for intensity images can provide valuable insights for denoising polarization images. Therefore, it is necessary to briefly review generic image denoising methods. However, it is not practical to cover all image denoising methods. Hence, this section focuses on a selection of image denoising algorithms that have provided guidance for subsequent polarization image denoising techniques.

3.1. Traditional Generic Image Denoising Methods

Traditional image denoising methods are the first to be applied to polarization image denoising, as they are extensions of grayscale and color image denoising techniques. According to the

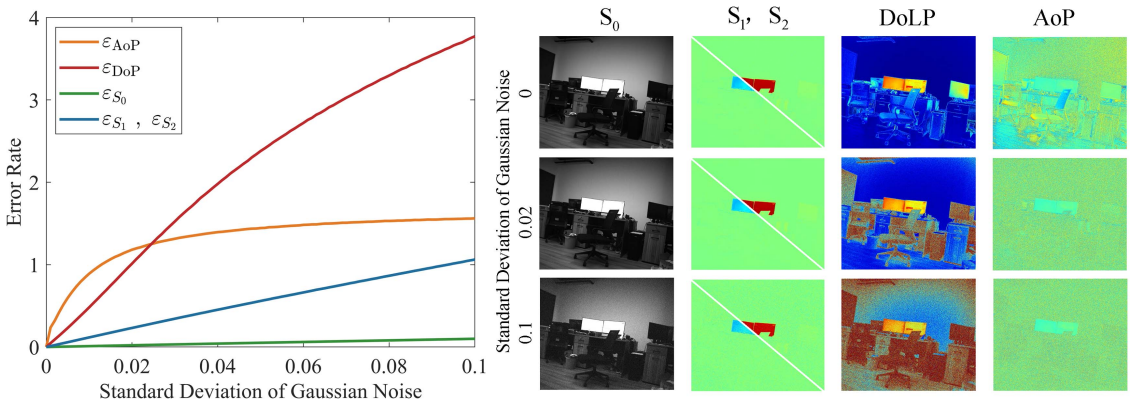

Fig. 3 Sensitivity of different polarization parameters. (a) Relationship between mean error rates and the standard deviation. (b) The computed Stokes parameters, DoLP, and AoP, with different variances.

classification method proposed by Goyal *et al.*[65], traditional image denoising methods can be divided into several categories: spatial domain filtering, transform domain methods, and sparse representation and dictionary learning methods.

A spatial domain filter can be categorized as either a local or non-local filter. Local filters denoise a pixel by considering surrounding regions, with the influence restricted by spatial proximity. Popular local filters designed for noise reduction include the Gaussian filter, bilateral filter, and Wiener filter. These methods efficiently remove noise but often fail to preserve image edges. Another approach within the spatial domain involves minimizing an energy function to compute the denoised image. A notable example is the TV method[66], which effectively preserves edges and details. However, TV-based methods may produce staircasing artifacts and require careful parameter selection. In contrast to local filters, non-local filters[67,68] utilize information from the entire image, offering greater robustness to noise. The non-local means (NLM) filter[69] is particularly influential; it applies weighted filtering based on non-local self-similarity priors to achieve image denoising. While non-local filters are effective in preserving edges and details while removing noise, they typically involve high computational complexity.

Due to the limitations of spatial domain techniques, researchers have increasingly turned to transform domain methods for image denoising. In the transform domain, both the image and noise exhibit distinct characteristics, allowing for effective noise suppression through filtering or thresholding methods[70]. The early development of these techniques stemmed from the Fourier transform, where denoising was achieved by designing a cut-off frequency. Since then, a variety of transform domain methods have been developed, including wavelet-based methods[71], principal component analysis (PCA)-based methods[72,73], and BM3D[74]. Among these, BM3D is particularly notable for its superior denoising performance, as it effectively combines transform domain filtering with non-local block matching. However, as noise levels increase, the effectiveness of BM3D diminishes significantly. Sparse representation[75] is another important denoising technique, valued for its ability to induce shift invariance. A prominent method in this category is K-singular value decomposition (K-SVD)[76], which removes noise while preserving details and textures using learned dictionaries. Despite its effectiveness, K-SVD can be computationally intensive, particularly when dealing with large patches.

3.2. *Generic Image Denoising Methods Based on Deep Learning*

Given the simplicity and effectiveness of deep learning, it has been widely embraced across various CNN denoising algorithms, resulting in a wide array of learning-based network variations[77,78]. According to the classification method proposed by Tian *et al.*[79], these methods can be summarized as two categories: single CNN and multiple CNNs for image denoising. Table 1 shows detailed information of these generic image denoising methods based on deep learning.

Single CNN denoising networks are the most common type. For instance, Zhang *et al.*[78,80] employed feedforward denoising convolutional neural networks (DnCNNs), integrating batch normalization (BN)[81], rectified linear unit (ReLU)[82], and residual learning[83] within the network architecture. Motivated by the achievements of the DnCNN, the prevalent ResNet neural network architecture was initially introduced by He *et al.*[84] in 2015 and has since found widespread application in various domains. This architecture effectively addresses the issue of vanishing gradients encountered in deep networks. In 2017, Huang *et al.*[85] introduced DenseNet, which mitigates gradient vanishing, enhances feature propagation, promotes feature reuse, and notably reduces parameter count through dense interconnections between layers. Inspired by ResNet and DenseNet, the residual dense network (RDN)[86,87], proposed by Zhang *et al.*, has demonstrated effectiveness across various image restoration tasks. Similarly, Park *et al.*[88] introduced a densely connected hierarchical image denoising network, which improved denoising performance by the modified U-Net, dense connectivity, and residual learning.

To make obtained denoisers mine richer features for complex scenes, CNNs with multiple sub-networks are conducted for image denoising. For example, to obtain comparative information for filtering noise, Zhang *et al.*[89] proposed a parallel and serial denoising network (PSDNet), which can well-balance the acquisition and purification of diverse features and can achieve an effective CNN for improving the effects of image denoising. To address limitations in the depth and width of lightweight CNNs, Zhang *et al.*[90] propose a multi-stage image DnCNN with wavelet transform (MWDCNN) for pursuing good denoising performance. Different from CNNs, the transformer can obtain effective structural information and can also achieve

Table 1 Summary of Generic Deep Learning Denoising Methods.

Method	Category	Application	Feature
DnCNN[78]	CNN	Image denoising, super-resolution, and deblocking	Feedforward denoising CNNs integrating BN, ReLU, and residual learning
RDN[86,87]	CNN	Image denoising, super-resolution, artifact reduction, and deblurring	An effective denoising CNN with advantages of ResNet and DenseNet
U-Net-based[88]	CNN	Gaussian image denoising and real noisy image denoising	A densely connected hierarchical image denoising network based on modified U-Net
PSDNet[89]	CNN	Synthesized noisy image and real noisy image denoising	An effective denoising CNN with parallel and serial structure
MWDCNN[90]	CNN	Gaussian noisy image and real noisy image denoising	A multi-stage image denoising CNN with the wavelet transform
CTNet[79]	CNN with Transformer	Synthesized noisy image and real noisy image denoising	Improving denoising in complex scenes by cross-transformer techniques
HWformer[91]	Transformer	Synthesized noisy image and real noisy image denoising	Long- and short-distance modeling by a heterogeneous window transformer
Noise2Noise[92]	CNN	Image denoising, Monte Carlo image denoising, and reconstruction of MRI scan	Training a blind denoiser by two noisy images from two snapshots
SSNet[93]	CNN	Image denoising and watermark removal	A perceptive self-supervised learning network for noisy image watermark removal
PSLNet[94]	CNN	Image denoising and watermark removal	Self-supervised learning network training a denoising CNN
U^2D^2Net[95]	CNN	Image denoising and dehazing	Unsupervised unified image dehazing and denoising network for a single image

promising results in denoising. For example, with long- and short-distance modeling ability, Lin *et al.*[91] proposed a heterogeneous window transformer (HWformer) to pursue better denoising performance. Therefore, Tian *et al.*[79] proposed a cross transformer denoising CNN (CTNet), which can extract more salient information by introducing transformer techniques in a CNN.

Due to the lack of real noisy images, various methods have been proposed to reduce dependence on large datasets. Self-supervised methods can obtain reference images according to the attributes of a given image. For example, Lehtinen *et al.*[92] used two noisy images obtained from two snapshots as noisy and reference images to train a blind denoiser. Tian *et al.*[93] proposed a parallel self-supervised network (SSNet) with attention mechanisms to remove noise. The above methods are all standalone denoising networks. In some cases, denoising networks are used as part of complex restoration tasks. For example, Li *et al.*[94] proposed a perceptive self-supervised learning network (PSLNet) for noisy image watermark removal, and the denoising network was used to improve the effects of image watermark removal. To remove the haze and suppress the noise simultaneously for a single hazy image, Ding *et al.*[95] designed an unsupervised network U^2D^2Net, which could restore the original information to the greatest extent.

4. Traditional Polarimetric Image Denoising Methods

The development of denoising techniques for polarized images can be roughly divided into three stages: The first stage involves the direct application of traditional image denoising algorithms. Although this can suppress noise to some extent, it is not ideal for restoring polarization information. The second stage involves specially designed methods for polarized images, utilizing image-prior models for noise removal. Considering the physical relationship between multiple channels, these methods excel at denoising Gaussian noise but perform poorly in real-world complex noise conditions. In the third stage, benefiting from advances in deep learning, denoising methods tend to integrate polarization characteristics with CNNs for noise suppression. These methods have become mainstream due to their powerful modeling capabilities, achieving significant denoising effects. This section mainly introduces the research status of polarization image denoising methods in the second and third stages, and analyzes their principles and characteristics.

In the first stage, the methods of suppressing noise in polarimetric images directly apply the aforementioned traditional denoising techniques. However, the inherent characteristics of polarimetric imagers impose limitations on the effectiveness of these algorithms. Therefore, more effective denoising algorithms specifically tailored to polarimetric images have emerged in the second stage. Three traditional image denoising methods, which are PCA-based[72], KSVD-based[76], and BM3D-based[74] methods, have become popular in the field of polarization imaging. Table 2 provides a detailed comparison of KSVD, PCA, and BM3D image denoising methods, highlighting their unique features, strengths, and weaknesses. Through specific design and improvements tailored to polarized images, these methods have achieved further effectiveness and can partially restore polarization information. Therefore, in the following sections, these representative traditional denoising methods designed for polarimetric images are discussed and compared.

Table 2 Comparison of KSVD, PCA, and BM3D Image Denoising Methods.

Method	Characteristic	Advantage	Disadvantage
KSVD	Dictionary learning-based approach; utilizes sparse representations	Effective for various types of noise; adaptable to different image structures	Requires training data; sensitive to parameter settings
PCA	Reduces dimensionality; identifies and retains major patterns	Good for Gaussian noise; simple implementation	Limited performance with complex noise; loss of fine details
BM3D	Groups similar image blocks; applies 3D transformation and filtering	Excellent at preserving details and textures; effective for various noise types	High computational complexity; requires tuning of multiple parameters

4.1. PCA-Based Polarimetric Image Denoising Method

PCA-based denoising[72,73] leverages the fact that the principal components represent the dominant patterns in the image, while the less significant components are often associated with noise. By retaining the major components and discarding the less important ones, PCA helps preserve the essential structure of the image while reducing the impact of noise.

Based on the PCA algorithm, Zhang *et al.*[34] proposed a polarimetric imaging denoising approach. Initially, training samples $\overline{\mathbf{X^n}}$ are extracted from variable blocks comprising intensity measurements oriented in four different directions. Subsequently, these training samples are transformed into the PCA domain $\overline{\mathbf{Y^n}} = \mathbf{P}\overline{\mathbf{X^n}}$, where $\mathbf{P}$ represents an orthonormal PCA transformation matrix. Denoising is performed in the PCA domain using $\widehat{\overline{\mathbf{Y^n}}} = \mathbf{C}_{\bar{\mathbf{Y}}}\mathbf{C}^{-1}_{\overline{\mathbf{Y^n}}}\overline{\mathbf{Y^n}}$, with $\mathbf{C}_{\bar{\mathbf{Y}}}$ and $\mathbf{C}^{-1}_{\overline{\mathbf{Y^n}}}$ denoting the covariance matrices. To obtain the denoised variable block, $\widehat{\overline{\mathbf{Y^n}}}$ is transformed back to the time domain, resulting in $\hat{\mathbf{I}} = (\mathbf{P}^T\widehat{\overline{\mathbf{Y}}}^n + E[\mathbf{X}^n])_{\text{center}}$, where the subscript "center" signifies the central 2-by-2 block of the variable block. Finally, the denoised single pixel value is computed by averaging the results from four adjacent center blocks. The denoising results of simulated and real polarimetric images are presented in Fig. 4, which shows the effectiveness of the PCA-based denoising method. Additionally, the peak signal-to-noise ratio (PSNR) results for different standard variances are shown in Fig. 4(c). After denoising, the values of PSNR are improved, whereas the performance decreases quickly with the increase of variance.

By leveraging the dimension reduction capability of PCA, it preserves the most pertinent aspects of polarimetric images while treating less relevant components as noise. Consequently, it excels at suppressing Gaussian noise of low magnitude. However, the trade-off is that the algorithm compromises on image details and edge information, making it less suitable for scenarios with substantial Gaussian noise.

4.2. KSVD-Based Polarimetric Image Denoising Method

The PCA-based denoising method can suppress Gaussian noise with a small magnitude. However, this enhancement comes with the drawback of significant loss of image detail, particularly around edges. As an alternative option, sparse representation has shown promising results in enhancing traditional grayscale/color images in recent years[75]. Sparse representation operates on the concept that every image patch can be represented as a linear combination of multiple patches from a dictionary that contains more elements than the patch itself. Numerous contemporary image denoising techniques leverage this sparsity prior exhibited by natural images[76], like KSVD-based methods.

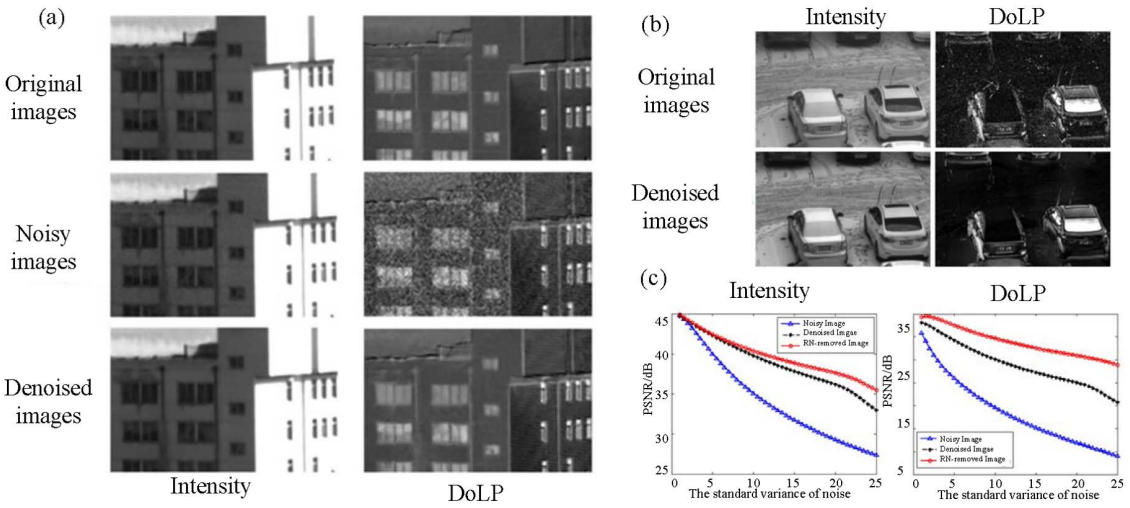

Fig. 4 Denoising performance of the PCA-based method. (a) Denoising results for the simulated noisy image; (b) denoising results for the real noisy image; (c) quantitative analysis results.

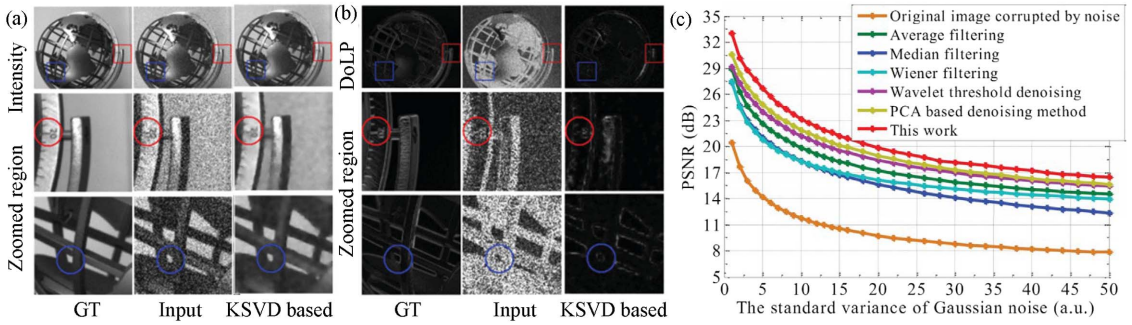

Fig. 5 Denoising performance of the KSVD-based method for Gaussian noise. (a) Intensity ($\sigma = 1$); (b) DoLP; (c) quantitative analysis results.

Ye *et al.* (2018)[36] introduced a denoising algorithm tailored for polarimeters, utilizing KSVD[96,97] and orthogonal matching pursuit (OMP)[98,99]. Its fundamental concept is searching for a dictionary for achieving optimized sparse representation of polarimetric image blocks by KSVD. Subsequently, the OMP is performed on noisy polarimetric image blocks for sparse decomposition. Therefore, finding the optimal dictionary D is of great significant, which could be expressed by

$$\min_{D,x} \|z^n - Dx\|_2^2 \quad \text{subject to} \quad \|x\|_0 \le T, \tag{13}$$

where x is the sparse matrix and z^n represents pixel vectors in I^n. The polarization signal component can be effectively represented as a sparse linear combination of these atoms, whereas the noise component, with its intrinsic randomness and lack of coherence properties, cannot. Leveraging the interrelationships among the four polarization channels ($I_0, I_{45}, I_{90}, I_{135}$), this approach significantly enhances image denoising performance, as demonstrated in Fig. 5.

In Fig. 5(c), the quantitative analysis results are presented. In terms of PSNR values, the KSVD-based method is 8.28% to 28.88% higher than other methods. Table 3 shows the restored polarization information obtained via polarimetric images, i.e., intensity (S_0), S_1, S_2, DoLP, and AoP images. Except for the AoP images, the metrics for other images have all improved, indicating that this method is not suitable for restoring AoP images, which are more sensitive to noise.

4.3. BM3D-Based Polarimetric Image Denoising Methods

Inspired by the concept of non-local and over-complete representation, in 2007, Dabov *et al*. introduced an approach combining spatial domain and 3D transform domain operation, known as BM3D[30]. As depicted in Fig. 6, the BM3D method operates by matching similar patches into 3D groups through block matching. These 3D groups are then transformed into the wavelet domain, where either hard thresholding or Wiener filtering is applied to suppress the noise. Subsequently, an inverse 3D transform is performed to obtain the denoised groups. Finally, putting the groups back according to the original position and aggregating the overlapped group, we can get the complete denoised image. An appealing feature of BM3D is its adaptability to color images, known as CBM3D[100]. It tailors BM3D for color images by applying BM3D separately to the three channels of the image in the YUV color space. Grouping is performed only once for the luminance channel (Y), and the same grouping is reused for the chrominance channels (U and V). This unique design of BM3D ensures efficient noise reduction across all color channels.

Table 3 PSNR Comparisons of Different Polarization Information.

Method	S_0	S_1	S_2	DoLP	AoP
Noisy input (dB)	18.61	18.58	18.58	4.71	3.84
K-SVD-based (dB)	28.97	30.99	33.00	22.58	4.24

While BM3D has demonstrated remarkable success in denoising tasks, it is not tailored to polarimetric images. In order to improve denoising performance on polarimetric images, Tibbs *et al*. proposed adapting the BM3D algorithm for use with polarimetric imaging, a method we call PBM3D[32]. PBM3D extends the principles of CBM3D by substituting the RGB to YUV transformation with a transformation from the camera component image $\mathbf{I} = (I_{0^\circ}, I_{45^\circ}, I_{90^\circ})$ to a selected polarization space, $\mathbf{P} = (P_0, P_1, P_2)$, denoted as $\mathbf{P} = \mathbf{T} \cdot \mathbf{I}$, and the transform matrix T can be obtained by

$$T = \arg\min_T \sum_i \|\mathbf{I} - \text{PBM3D}(\mathbf{I^n})\|^2, \tag{14}$$

where $\mathbf{I^n}$ represents $\mathbf{I}$ with Gaussian noise added. The denoising performance in Fig. 7(a) shows the effectiveness of PBM3D, and denoised images using PBM3D are notably faithful to the original. Then in Fig. 7(b), the PSNR values for the same image as shown in Fig. 7(a) are compared. It shows that the PBM3D method outperforms other methods at every noise level, and it is on average 0.84 dB higher than the second-best method.

In 2018, Abubakar *et al.*[35] introduced a denoising method specifically designed for a division of focal plane (DoFP) imaging system, named BM3D-DoFP. In the initial stage, the algorithm is similar to BM3D and performs similar block matching. It ensures that these patches incorporate all four intensity measurements equally to fully leverage the inter-relationship among the four distinct polarization channels. Then, just like the BM3D method, it applies hard thresholding and subsequently repeats the same procedure as the initial stage, with the exception of utilizing Wiener filtering instead of hard thresholding. Similarly, in 2022, Liang *et al.*[33] extended the BM3D

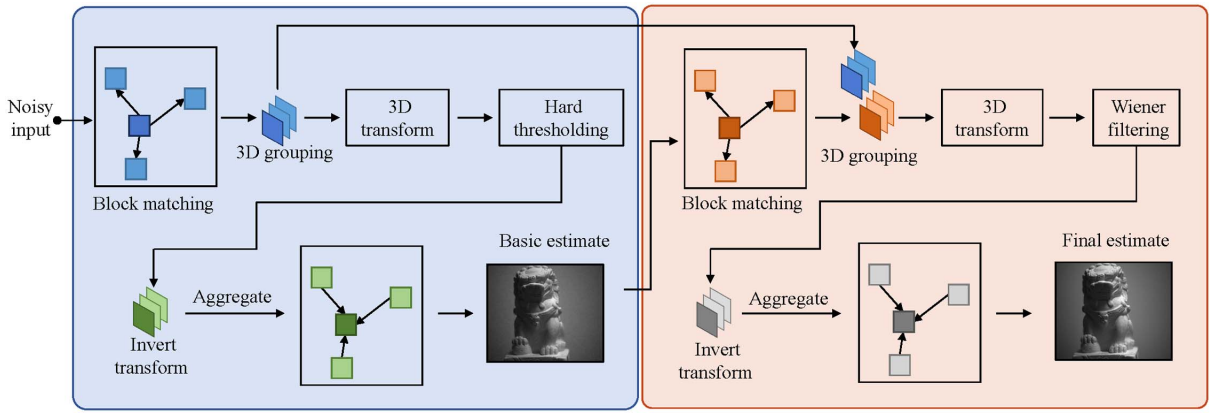

Fig. 6 Flow chart of the BM3D algorithm.

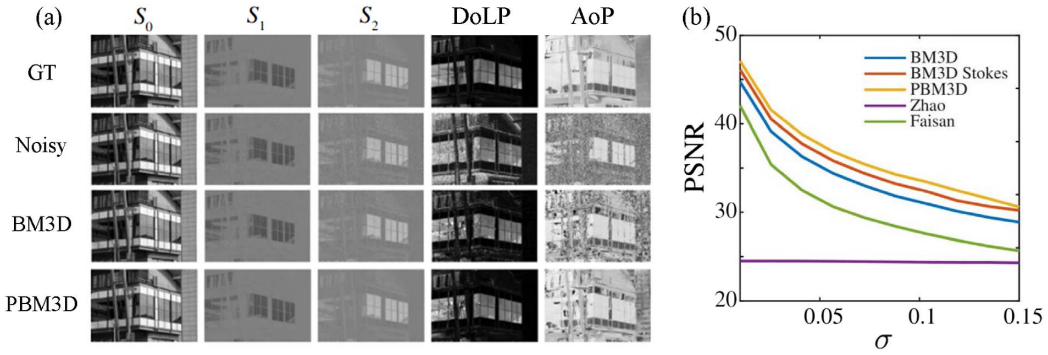

Fig. 7 Denoising performance for Gaussian noise. (a) Polarization components after applying PBM3D methods ($\sigma = 0.026$); (b) quantitative analysis results.

method to color polarimetric image denoising. It mainly restores all the 12-channel $[(R, G, B) \cdot (0°, 45°, 90°, 135°)]$ images from a color polarization filter array (CPFA) image dataset. This study first demonstrates the correlation between the newly added color channel and the polarization direction channel. The proposed algorithms leverage the inter-relationship between the various polarization channels, allowing them to be applied to the superpixel and achieve superior noise suppression performance.

However, the denoising algorithms described in most studies share a common characteristic: they are designed specifically to address Gaussian noise. Nevertheless, real-world polarimetric images are often affected by other kinds of noise that can significantly impact imaging quality. In 2021, Abubakar *et al.*[37] explored an alternative form of noise, referred to as "speckle noise," and introduced an adaptive algorithm leveraging the BM3D framework. They introduced an adaptive approach that improved the collaborative filtering. According to the smoothness of the matched block, it decides whether to employ hard thresholding or soft thresholding. In regions with significant noise levels, it adopts the original hard thresholding approach. In smoother regions with lower noise levels and richer image texture, this method adopts soft thresholding. This ensures effective filtering of speckle noise while preserving critical image details. The proposed algorithm demonstrates superior efficacy in attenuating speckle noise in polarimetric images.

5. Learning-Based Polarimetric Image Denoising Methods

Image denoising has greatly benefited from advancements in deep learning, especially CNNs designed specifically for image processing. DNNs have leveraged the powerful and flexible nonlinear fitting capability to achieve remarkable performance in various vision tasks, with image denoising being one of the prominent applications[101,102]. The success of learning-based methods in various applications has demonstrated their effectiveness in extracting image structures and features[103]. Deep learning, in particular, exhibits significant advantages for image recovery in challenging and noisy environments compared to traditional methods[104,105]. Therefore, applying this technique to remove noise and extract polarimetric features in polarimetric images is promising, especially for those polarimetric parameters that are more sensitive to noise.

The domain of deep polarimetric image denoising has undergone rapid development, but in a somewhat disjointed way. As illustrated in Fig. 8, a multitude of denoising approaches have emerged in recent years. This motivates us to conduct a comprehensive review of recent advancements in this research domain, aiming to offer an overview of current methodologies and insights into potential research directions.

As illustrated in Fig. 8, the synthesis or connection between polarimetric imaging and deep learning has two aspects. In the

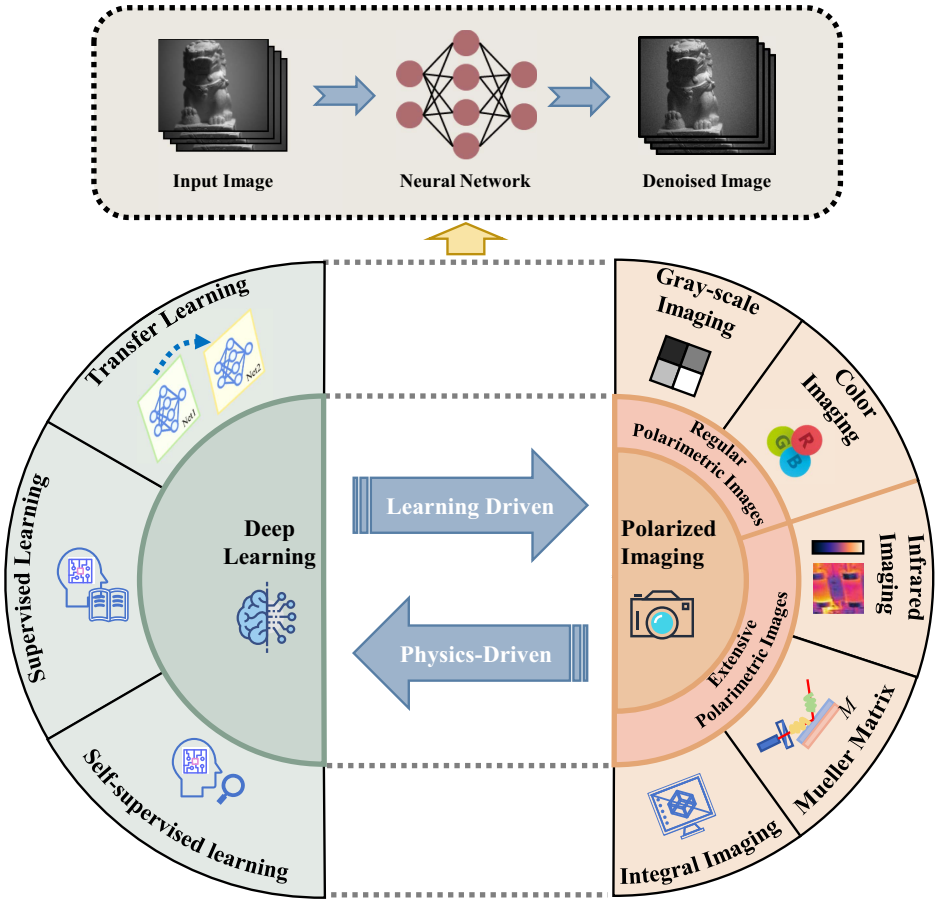

Fig. 8 Synergy between polarimetric imaging and deep learning techniques.

realm of deep learning, the primary approach involves training a mapping relationship from noisy images to clean images through supervised learning. Early CNNs operated primarily under this paradigm. This supervised approach achieves excellent denoising results through extensive dataset training, but its performance is constrained by the quantity and quality of the dataset. To mitigate the model's reliance on datasets, the researchers developed transfer learning (TL) methods. TL transfers knowledge from a source domain with large datasets to a target domain lacking sufficient data, thus reducing the requirement for datasets. In addition, there are unsupervised methods that do not require paired label images, such as those employing generative adversarial networks (GANs) for image denoising. While TL and unsupervised learning reduce training costs, their denoising performance may deteriorate compared to supervised learning due to a lack of data support.

In the field of polarization imaging, advances involve leveraging multiple data sources to support deep learning or integrating various optical techniques to mitigate noise. Inspired by Ilesanmi *et al.*[47], in this review, we broadly divide polarization imaging methods into two categories: regular polarization imaging and extensive polarization imaging. Regular polarization imaging refers to grayscale and color polarization imaging, forming the basis of polarization imaging. It benefits from deep learning methods for noise suppression and restoration of polarization information. To address the degradation in polarization image quality due to noise, optical methods can provide compensation. Infrared imaging, for example, uses thermal radiation detection to achieve relatively high-quality images in low-photon environments. Integral imaging (InIm) captures multiple angles to enhance scene information and improve image SNR. In addition, techniques such as Mueller matrix imaging and remote sensing polarization imaging complement polarization imaging, synergistically enhancing overall effectiveness.

In summary, there exists a promising synergy between polarimetric imaging and deep learning techniques. Polarimetric imaging techniques and their associated applications facilitate the advancement of deep learning by continuously developing physics-driven models. The integration of optical information can endow deep learning technology with more explicit physical significance and inject new vitality into the advancement of deep learning techniques. Conversely, deep learning enhances polarimetric imaging by improving the capability and performance of optical technology through learning-driven approaches. Through deep learning technology, obtaining high-quality polarization images and polarization information has become simpler and easier, greatly promoting the application of polarization imaging technology in many fields. Integration of deep learning and polarimetric imaging techniques may offer solutions to various challenges and desired functionalities in both domains.

In recent years, deep learning methods have also been effectively applied in polarimetric imaging[52,106–108]. In contrast to

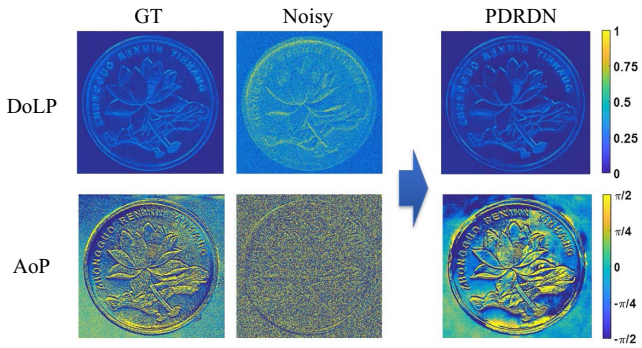

Fig. 9 Learning-based denoising for grayscale polarimetric images[39].

most existing denoising networks, which only fuse information from the spatial domain, these methods explicitly consider polarization information and remove noise. Designing network architectures to fully exploit polarization is important for polarimetric image denoising. In the following sections, we will introduce denoising networks specifically designed for polarimetric images according to the classification shown in Fig. 8.

5.1. Denoising for Typical Polarimetric Imaging

5.1.1. Grayscale polarimetric image denoising

In 2018, Li *et al.*[39] first considered the Stokes imager as an example to demonstrate that the employment of DNNs has demonstrated the capability to effectively suppress noise in polarimetric images and enhance their overall quality. A denoising network called PDRDN is designed, and its structure is based on RDN. This neural network takes a polarization image with four angles as input and generates the residual between the input and prediction image as output. Because polarization is considered and the network structure is efficient, the recovered image has perceptually pleasing results, as shown in Fig. 9. Furthermore, the efficacy of this approach on various materials has been validated. This represents the initial investigation into denoising polarimetric images using deep learning. These findings underscore the benefits of integrating polarization information and constraints into the network, resulting in enhanced denoising performance.

Table 4 Average PSNRs (dB)/SSIMs of Different Methods.

Method	S_0	DoLP	AoP
Input	22.24/0.602	10.70/0.123	9.64/0.054
BM3D	25.93/0.890	17.52/0.766	13.27/0.159
PDRDN	32.53/0.967	23.89/0.808	16.34/0.224
CARDN	31.65/0.923	27.04/0.843	20.27/0.249

The PDRDN denoising algorithm is suitable for image restoration in complex and high-noise environments. However, the result still contains some artifacts, especially in AoP images. To enhance denoising performance further, a channel attention-based residual dense network (CARDN) was introduced by Liu *et al.*[43], aiming at removing noise and restoring polarization information in polarimetric images. The network leverages a novel channel attention residual dense block (CARDB) to highlight informative features while suppressing less relevant ones. The structure of CARDN is shown in Fig. 10. In particular, they investigate the underlying mechanism of channel attention[109], and the visualization of explanation intuitively shows that channel attention can enhance the denoising effect by emphasizing informative features and suppressing noisy features. Adaptive polarization loss is also designed to guide the network to focus on polarization information. Figure 10(c) illustrates denoising outcomes for various polarization parameters (i.e., intensity, DoLP, and AoP) obtained by different methods. It is evident that CARDN exhibits superior performance across all polarization parameters, effectively restoring all image details. Particularly in AoP images, the noise reduction appears notably enhanced. Furthermore, in Table 4, we compare several methods (i.e., BM3D, PDRDN, and the proposed CARDN) using PSNR and structural similarity index (SSIM). Deep learning methods like CARDN significantly outperform traditional methods such as BM3D, particularly in improving the quality of DoLP and AoP images. Compared to BM3D, CARDN achieved a 2.4-fold (PSNR) improvement in DoLP and a 2.9-fold improvement in AoP.

Deep learning was used for denoising polarimetric imaging, and near-optimal performance was achieved to remove the noise of polarimetric parameters. However, the deep learning method relies on massive training data because it needs large datasets to

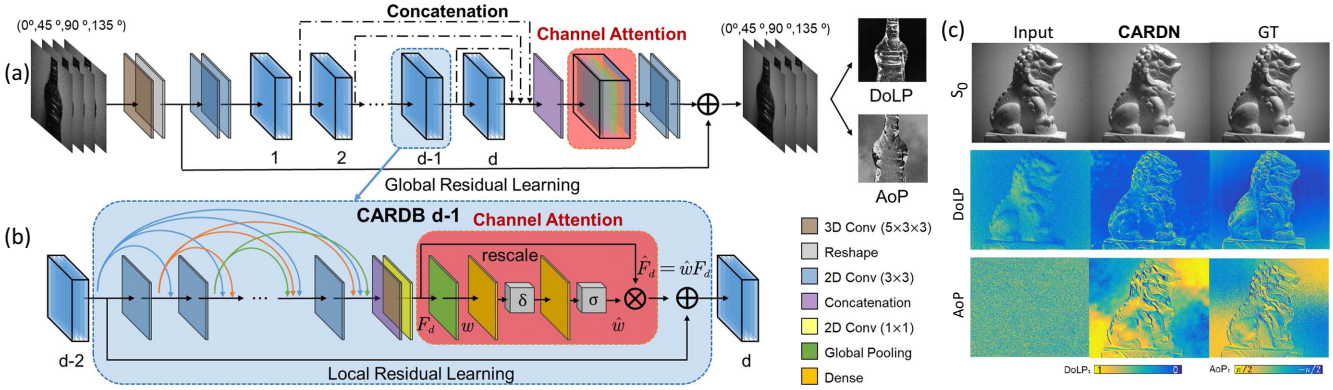

Fig. 10 Learning-based denoising for grayscale polarimetric images[43]: (a) network architecture; (b) channel attention residual dense block; (c) restored results comparison.

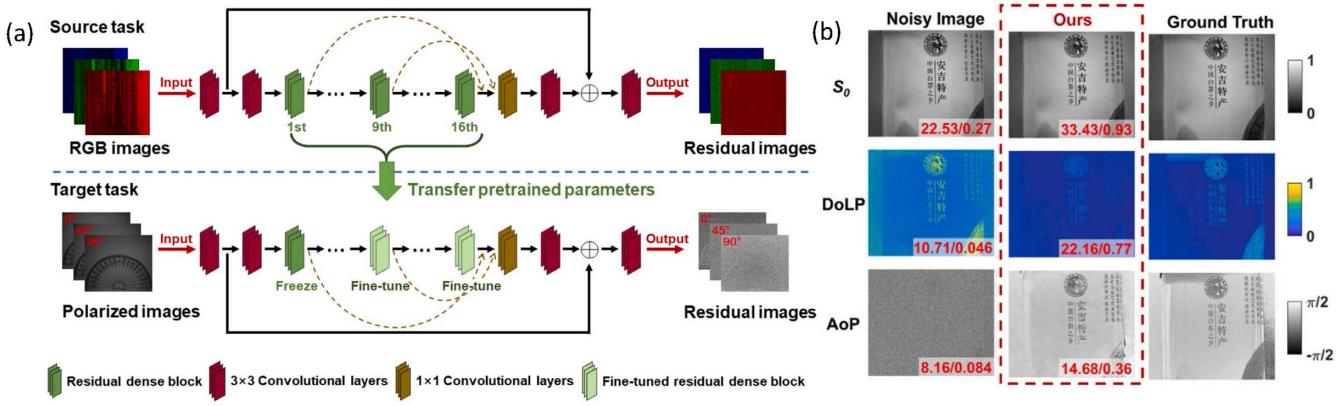

Fig. 11 Transfer-learning-based denoising for polarimetric images[46]: (a) the pipeline of the transfer-learning-based method; (b) visual comparison for denoising performance.

learn the knowledge for specialized tasks. Therefore, for deep learning methods of polarimetric imaging denoising, a large amount of data is required to achieve satisfactory performance. This could be a critical limitation for this method because large-scale datasets are not always available, especially for polarimetric images.

TL[110,111] is a learning-based approach aimed at addressing the issue of insufficient training image data. By leveraging knowledge from a source domain with sample data, TL transfers this knowledge to a target domain suffering from a scarcity of data. Therefore, TL is widely used in many fields in which it is difficult to get a large amount of data and brings significant positive effects, such as face recognition[112], image classification[113], and object detection[113]. Therefore, we believe introducing TL to polarimetric imaging can break the limitation of the dataset scale and effectively achieve the denoising of polarimetric images based on a small amount of data. However, utilizing TL directly for polarimetric imaging poses a challenge as polarization information is multi-dimensional and highly susceptible to noise.

To effectively tackle these challenges, it is crucial to meticulously design the network architecture and optimize the loss function. As shown in Fig. 11(a), Hu *et al.*[114] applied the deep TL approach to the polarimetric image denoising field. In particular, to increase network transferability, real-world color image denoising is chosen as the source domain, and a polarimetric image dataset containing images of different materials and environments is constructed. The noise levels of these images vary by changing the exposure time[115]. The pre-trained partial network is reused in the color image denoising domain, and the polarimetric denoise model is fine-tuned through a small polarimetric image dataset. Figure 11(b) illustrates that the proposed TL-based method is effective in noise removal and polarization detail recovery in polarimetric images, achieved by training the denoising model on a small-scale polarimetric dataset. Additionally, the values of the PSNR (dB)/SSIM are presented in Fig. 11(b). The TL algorithm significantly improves the quality of all three types of images, with the most dramatic enhancements observed in the DoLP image, especially in terms of the SSIM, which is increased by approximately 16.74 times.

As depicted in Fig. 12(b), CNN-based methods usually necessitate a substantial number of noisy-clean training image pairs for supervised learning. However, acquiring such pairs can be challenging and labor-intensive, as obtaining clean images often involves extended exposures under specific conditions

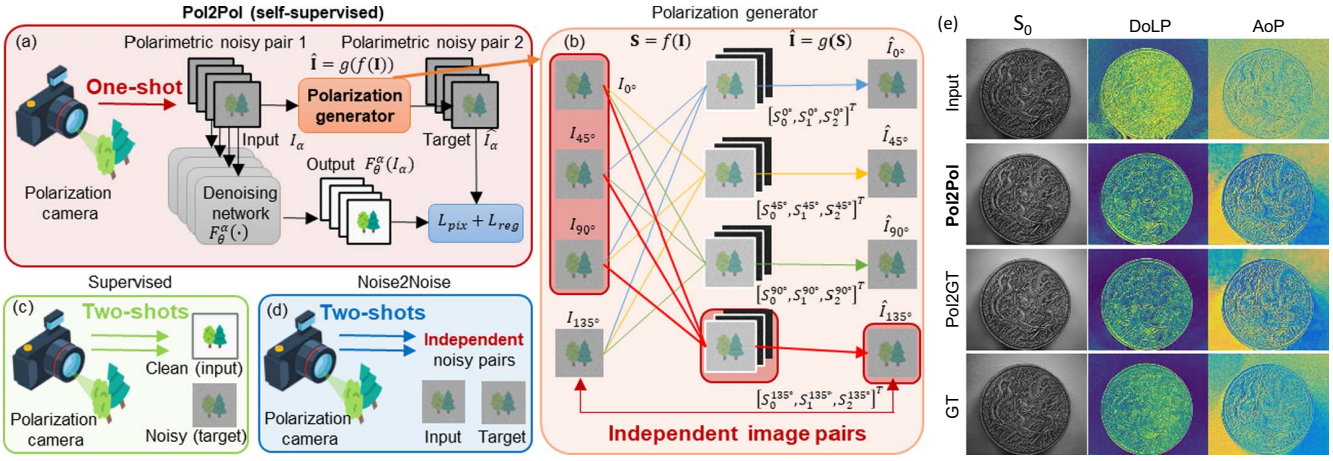

Fig. 12 Self-supervised-based denoising for polarimetric images[116]: (a) the pipeline of Pol2Pol; (b) the detail of the polarization generator; (c) the pipeline of supervised learning; (d) the pipeline of the Noise2Noise method; (e) visual comparisons of different denoising methods.

Table 5 Average PSNRs (dB)/SSIMs of Pol2Pol and Pol2GT.

Method	S_0	DoLP	AoP
Input	23.50/0.707	15.54/0.122	12.51/0.112
Pol2Pol	27.72/0.874	23.34/0.720	16.00/0.325
Pol2GT	27.95/0.880	23.61/0.723	16.11/0.328

within the same static scene[117]. Instead of using clean images, Noise2Noise[92] leverages pairs of noisy images captured from identical scenes, and it proves that training the network with multiple independent noisy images per scene is equivalent to noisy-clean image pairs, as shown in Fig. 12(c). Based on Noise2Noise, various self-supervised denoising methods are proposed, such as Noise2Void[118] and Blind2Unblind[119]. To create viable training pairs from individual noisy images, these techniques strive to produce two separate noisy images derived from a single noisy image. For instance, Neighbor2Neighbor[120] suggests training the network using sub-sampled pairs extracted from the same noisy image. Nonetheless, these denoising approaches primarily rely on data from a single image, leading to constrained performance. Furthermore, without incorporating polarization information, these methods suffer degradation when handling noisy polarimetric images.

Motivated by Noise2Noise, Liu *et al.*[116] proposed a self-supervised polarimetric image denoising framework named polarization to polarization (Pol2Pol), shown in Fig. 12(a). Pol2Pol requires only one-shot noisy image per scene, and each training pair is synthesized from the one-shot noisy image, based on polarization relationships. Figure 12(d) shows a two-step polarization generator, which generates independent noisy training image pairs by specific design. First, selecting an angle, a group of Stokes vectors is calculated using the remaining three angles. Second, according to the Stokes relationship, the image of the selected angle can be generated. Repeating the steps for each angle, the noisy polarimetric image pairs can be obtained. In Fig. 12(e), it is evident that Pol2Pol delivers competitive results comparable to supervised methods (Pol2GT), which demand more extensive training data. Furthermore, by quantitatively analyzing the results in Table 5, we find that the values of Pol2Pol2 are slightly lower than those of Pol2GT, which is reasonable. This is because, compared to supervised learning, self-supervised learning utilizes less data information.

5.1.2. Color polarimetric image denoising

Color polarimetric imaging can capture both the color and polarization properties of light, which enriches the preserved information and provides a more faithful representation of the target[121,122]. However, as discussed in Sec. 2, some essential polarimetric parameters are susceptible to noise, and denoising methods also play an important role in color polarimetric images. Unlike denoising grayscale polarimetric images, denoising color polarimetric images is more challenging. The main reason is that color polarimetric images have multiple dimensions, including space, color, and polarization, and the growth of dimensions places greater demands on denoising. Therefore, such algorithms[123] designed for conventional images cannot be applied directly.

Unlike color images, which have independent (R, G, B) channels, polarimetric images have physical correlations between different polarization channels. Because the implicit physical correlation in the polarization dimension is excessively complex, effectively exploiting the correlation between dimensions and restoring precise physical information from noisy polarimetric images remains a challenge. Indeed, the development of denoising algorithms tailored specifically for polarimetric images is crucial.

To denoise color polarimetric images, a common strategy is to decompose multi-dimensions into various components. Hu *et al.*[38] introduced IPLNet, a hybrid network designed to improve the quality of both intensity and polarization images concurrently. The network architecture and loss function were tailored to balance the imaging performance of intensity and polarization data. Specifically, IPLNet decomposes RGB channel dimensions into three branches, and then denoises each channel (i.e., (R, G, B) color channels). While effective for indoor and outdoor datasets, the method suffers from computational intensity due to its large parameter count. Additionally, there are inaccuracies in color representation in some areas of the enhanced S_0 map, as depicted in Fig. 13(b).

ColorPolarNet[42], introduced by Xu *et al.*, could handle the multi-tasking of color polarization imaging. Both intensity (RGB) and polarization information could be enhanced by this network. ColorPolarNet is also inspired by RDN, and the core

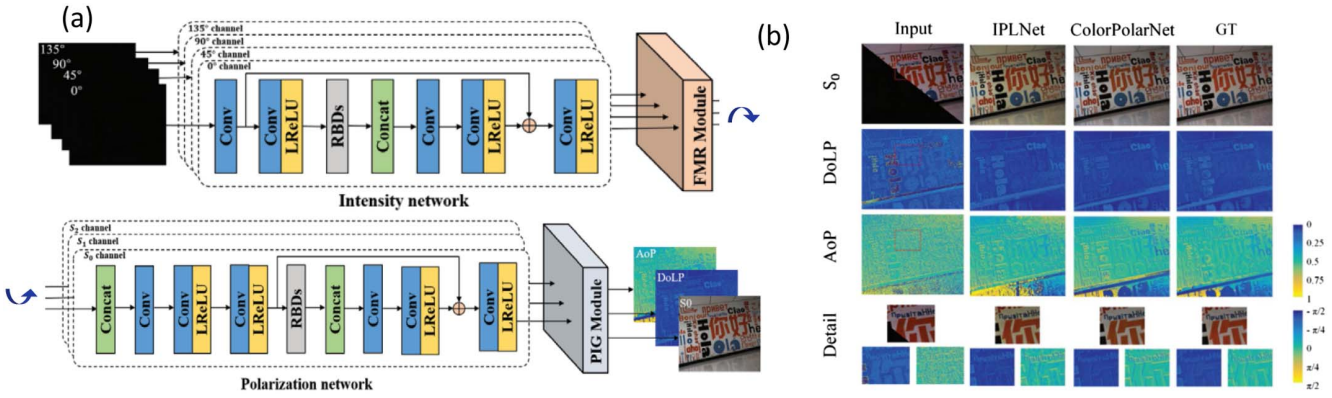

Fig. 13 Learning-based denoising for color polarimetric images[43]: (a) network architecture of ColorPolarNet; (b) restored result comparison of IPLNet and ColorPolarNet.

of RDN is residual density blocks (RDBs). Unlike IPLNet, ColorPolarNet uses a two-step network design to decompose channel and polarization dimensions. As shown in Fig. 13(a), it first processed the intensity part individually, restored the color information by an intensity network, and then restored the polarization information by a polarization network. As illustrated in Fig. 13(b), ColorPolarNet is effective in denoising color images and polarization information images. Additionally, it improves the structure of modules; therefore, it exhibits higher operational efficiency compared to IPLNet. Color polarimetric images strongly correlate different polarization channels, which have explicit physical significance. Therefore, in order to achieve the enhancement of color polarimetric images, we need to fully exploit the intrinsic physical correlation between dimensions, which is instructive for restoring high-quality polarization information.

Inspired by 3D convolution[124], Liu *et al.*[44] proposed a 3D convolutional neural network (3DCNN) with an entirely 3D architecture for denoising color polarimetric images, and the network is shown in Fig. 14(a). In this method, 3D convolutions are applied to extract information from multiple dimensions, i.e., space, color, and polarization, as shown in Fig. 14(b). By jointly extracting features related to space, color, and polarization, 3DCNN can effectively incorporate coherence across different dimensions. In Fig. 14(c), we compare the denoising performance of IPLNet, ColorPolarNet, and 3DCNN. Experimental results show that the 3DCNN-based method can remove noise while maintaining color and polarization information simultaneously. IPLNet and ColorPolarNet did not fully consider the correlation between space, color, and polarization, and independent processing of each dimension extracts information only spatially. As a result, it is difficult to obtain the desired color polarimetric images.

Table 6 Average PSNRs (dB) and SSIMs of Different Color Polarimetric Image Denoising Methods.

Method	S_0	DoLP	AoP
Input	20.24/0.605	14.37/0.180	8.42/0.096
CBM3D	25.45/0.805	17.87/0.419	10.33/0.157
IPLNet	27.54/0.841	24.33/0.558	14.57/0.277
ColorPolarNet	33.24/0.937	24.12/0.513	14.94/0.286
3DCNN-based	33.44/0.948	25.94/0.706	17.18/0.310

Based on the data provided by Liu *et al.*[44], we give some quantitative analysis results of different denoising methods for color polarimetric images in Table 6. From this table, we can find that, for S_0, DoLP, and AoP images, the 3DCNN-based method outperforms other methods in terms of PSNR and SSIM, which verifies the feasibility of applying 3D convolutions to improve the denoising performance.

Recent research has shown that vision transformers (ViTs)[125–127] have enormous potential to explore global context interactions and outperform CNNs in a variety of imaging problems. Embracing the development of ViTs, Li *et al.*[46] introduced a ViT approach tailored for denoising color polarimetric images. The network adopts a four-stage U-Net architecture, as illustrated in Fig. 15(a), where each stage incorporates successive hybrid transformer blocks to handle deep features. Unlike traditional image denoising tasks, polarimetric color image denoising seeks to recover intensity information while maintaining accurate polarization information. Based on the above considerations, the proposed hybrid transformer block can capture spatial[128] and channel[129] attention for better

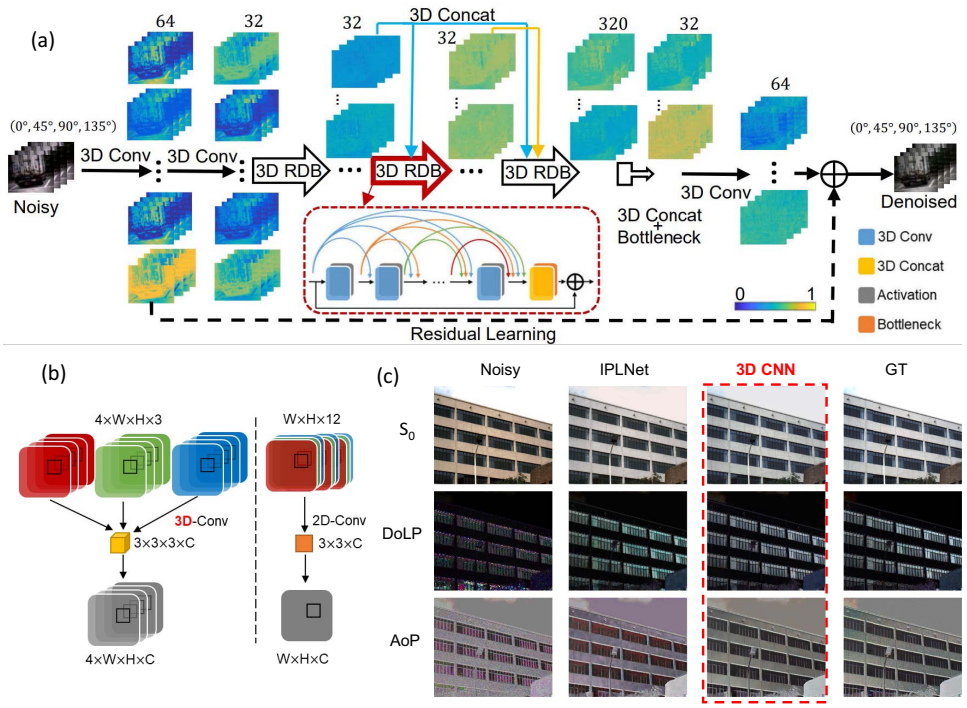

Fig. 14 3D CNN-based denoising method[43]: (a) network architecture; (b) comparison of 2D and 3D convolutions; (c) restored results.

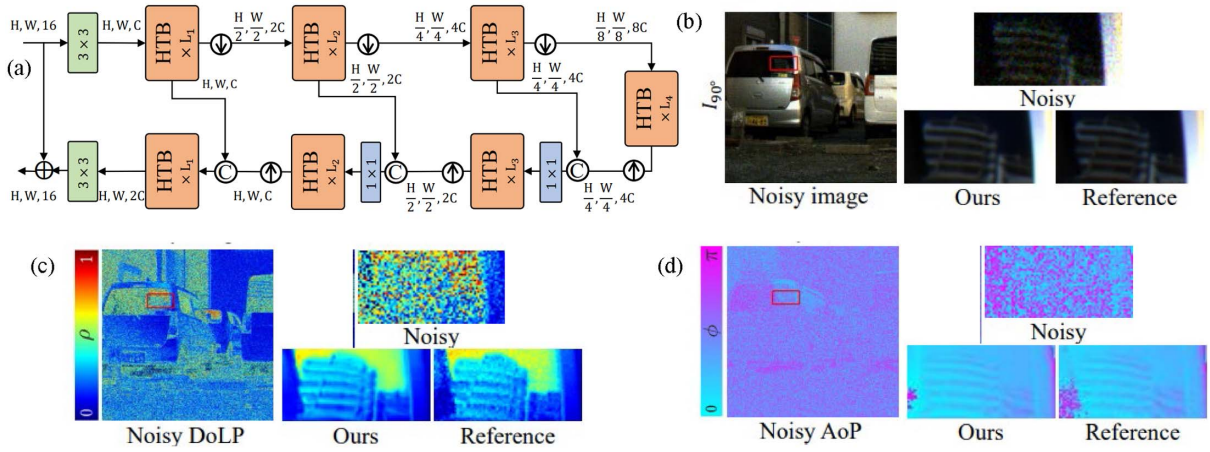

Fig. 15 Transformer-based denoising for color polarimetric images[46]: (a) the pipeline of the transformer-based method; (b)–(d) visual comparison of polarimetric color image denoising.

denoising performance. It is also expected to model channel interconnections and explore the polarization priors that exist implicitly in the channel dimension. The visual comparison depicted in Fig. 15(b) illustrates the effectiveness of transformer-based methods compared to traditional approaches. While traditional methods manage to reduce noise to some extent, they often fail to reconstruct polarization information accurately. In contrast, transformer-based methods not only remove noise but also restore textures in S_0, DoLP, and AoP information.

From the above methods, we find that a deep learning network with polarization knowledge is effective for noisy image enhancement and polarization information restoration. Table 7 shows a summary of the above research.

5.2. Denoising for Extensive Polarimetric Imaging

5.2.1. Infrared polarimetric image denoising

In scenarios with limited photon availability, such as low-light conditions, visible polarimetric images are easily corrupted by noise following a Gaussian distribution. Conversely, polarimetric images captured in the long-wave infrared (LWIR) spectrum benefit from sufficient thermal photons[16,130,131]. As a result, LWIR imaging detectors are frequently applied to capture polarimetric information in such cases. Infrared polarization imaging technology has demonstrated remarkable efficacy compared to typical infrared imaging across different applications, including contrast adjustment[132], camouflage target detection[133], and interference-resistant detection[134]. However, polarization images acquired in these scenarios are inevitably marred by diverse noise sources, exacerbated by the typically lower spatial resolution of infrared images. Consequently, denoising and demosaicking processes are imperative for enhancing the quality of infrared polarimetric images.

For denoising LWIR DoFP images, in 2023, Li *et al.*[45] introduced a network, termed PJNDNMNet. This method integrates Poisson-Additive-Stripe mixed noise level estimation[135] to guide the denoising process. Based on the fact that the deep learning method could learn the features and characterization of LWIR polarimetric images, they developed a three-step progressive CNN architecture for addressing image enhancement tasks, as depicted in Fig. 16(a). In addition, a Poisson-Additive-Stripe mixed noise level estimation technique is proposed. In order to separate stripe noise from other sources, the polarization measurement redundancy error map[136,137] is utilized, thereby improving the accuracy of mixed noise level estimation. Hence, accurate estimation of noise levels in real LWIR DoFP images is obtained by this innovative estimation approach. As a result, the generated training data closely

Table 7 Summary of Learning-Based Denoising Methods for Typical Polarimetric Images.

Method	Category	Application	Highlight
PDRDN[39]	Supervised	Grayscale	Modified RDN for polarimetric image denoising
CARDN[43]	Supervised	Grayscale	Channel attention and adaptive polarization loss
TL[114]	Supervised	Grayscale	Recovering polarization information with a small-scale polarimetric dataset
Pol2Pol[116]	Self-supervised	Grayscale	Conducing paired images by the Stokes relationship
IPLNet[38]	Supervised	Color	Decomposing color polarization images into 12 channels by three sub-networks
ColorPolarNet[42]	Supervised	Color	Decomposing color polarization images into intensity network and polarization network with the Stokes vector
3DCNN[44]	Supervised	Color	Processing high dimensions of color polarization by 3D convolution
ViT-based[46]	Supervised	Color	Exploiting polarization correlation by the transformer block

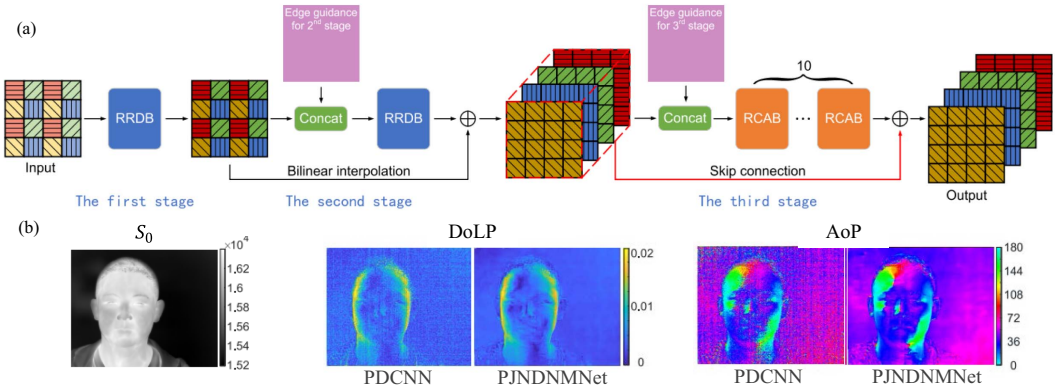

Fig. 16 Learning-based denoising for infrared polarimetric images[46]: (a) the architecture of PJNDNMNet; (b) visual results for infrared polarimetric image denoising.

resembles real-world scenarios, facilitating better adaptation of the trained network to real scenes. This improvement is illustrated in Fig. 16(b). In 2023, Fan *et al.*[16] proposed a multi-path network for LWIR polarization imaging-based road detection techniques. This method contains a prepossessing module, which has a BM3D and a polarization difference model to denoise and demosaic, respectively. The denoising of LWIR polarization images could improve the quality of polarization information, thereby enhancing the accuracy of subsequent road detection.

5.2.2. Integral polarimetric image denoising

InIm stands out as a prominent 3D imaging technique, particularly advantageous for enhancing scene visualization in noisy conditions[138,139]. In InIm, the 3D representation of a scene is acquired by capturing 2D images from various imaging angles, followed by a computational or optical reconstruction process. The utilization of various angles of 2D images for 3D image reconstruction enables the capture of depth or distance information, and optimally enhances noisy imaging performance in a maximum likelihood sense[140].

In 2021, Usmani *et al.*[40] adopted the DnCNN[78] for visualizing objects in noisy environments by combining it with passive polarimetric InIm under low-light conditions, as illustrated in Fig. 17(a). In degraded environments, the DnCNN is applied to improve the imaging quality of polarimetric imaging. Notably, rather than directly outputting the denoised image, the network formulated a loss function to estimate the residual noise image at each pixel, which represents the difference between the predicted clean image and the input noisy image. Experimental optical investigations demonstrated that integrating the DnCNN with 3D polarimetric imaging is effective in mitigating noise arising from photon-starved conditions and camera noise, thereby improving polarimetric 3D imaging, as depicted in Fig. 17(b). Table 8 shows the SNR of 2D/3D polarimetric images under different noise levels by adjusting photons/pixels. The quantitative comparison demonstrates that the DnCNN method provides a significant improvement in SNR

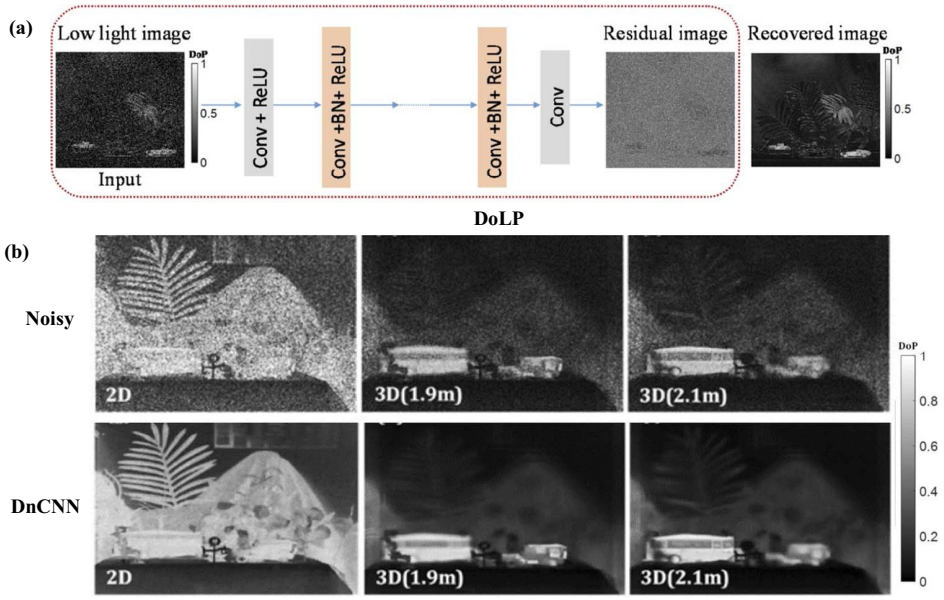

Fig. 17 DnCNN-based denoising method for integral polarimetric imaging[40]. (a) The structure of the DnCNN. (b) Restored results of the DoLP.

Table 8 Quantitative Analysis Results of the DnCNN-Based Method in Different Noise Levels.

Noise Level (Photons/pixel)	Noisy polarimetric images		Recovered polarimetric images using DnCNN	
	2D DoLP image (SNR) (dB)	3D DoLP image (SNR) (dB)	2D DoLP image (SNR) (dB)	3D DoLP image (SNR) (dB)
0–4	0.06	0.23	0.51	2.79
4–8	0.11	1.24	0.92	6.74
8–12	0.70	3.32	3.80	10.01
12–16	2.23	6.13	11.70	21.63
16–20	2.91	7.69	15.78	23.23

for both 2D and 3D DoLP images across all noise levels. 2D/3D DoLP images see an average improvement of approximately 5.6/4.4 times. The largest improvement is observed at the lowest noise level (0–4 photons/pixel), with the 3D DoLP image SNR improving by over 11.1 times.

5.2.3. Mueller matrix polarimetric image denoising

The Mueller matrix offers a comprehensive insight into a sample's polarization characteristics, rendering it highly responsive to microstructural features at scales smaller than the wavelength of light. Among the available tools for analyzing Mueller matrices, the Mueller matrix microscope has demonstrated encouraging applications in biomedical research and clinical settings[18,141]. While denoising methods based on machine learning have previously achieved success in cleaning intensity images obtained through polarization cameras in the Stokes framework, it is crucial to recognize that the intricacies of the Stokes framework differ notably from those of the Mueller framework[142,143].

In 2022, Yang *et al.*[41] devised the Mueller denoising U-Net (MDU-Net), which integrates channel attention mechanisms with a deep residual U-Net architecture. They accomplished denoising by training the MDU-Net with a substantial dataset comprising paired noisy and clean Mueller matrix images. These images were acquired using a Mueller matrix microscope equipped with both a rotating polarizer and a rotating wave plate polarization state generator. The MDU-Net architecture follows the typical U-Net structure[144,145], comprising encoder and decoder blocks, as illustrated in Fig. 18(a). At each decoder stage, original U-Net structures directly fuse features in different levels with skip connections. Unlike U-Net, MDU-Net tries to exploit the correlations between channels in different network stages before fusing, achieved through a channel attention mechanism[146]. This mechanism enables the model to prioritize relevant information, resulting in effective noise reduction in Mueller matrix images across different magnifications and generalization to samples beyond the training dataset. The denoising of Mueller matrix images also leads to enhanced contrast in polarization-based parameter images, particularly benefitting polarimetry basis parameters, as demonstrated in Fig. 18(b). Then in Table 9, the mean root mean square error (MRMSE), mean PSNR (MPSNR), and mean SSIM (MSSIM) are used to evaluate the denoising performance on the images reported in Ref. [41]. After the MDU-Net, the image quality shows significant improvement compared with the noisy images.

For extensive polarimetric imaging, modified CNNs are effective in removing the Gaussian noise and real noise with the help of extra optical information. Table 10 displays a summary of these denoising methods.

6. Discussion

Table 11 summarizes these methods, facilitating comparison and aiding researchers in selecting appropriate techniques for their specific applications. By comparing these denoising methods, we can find that learning-based methods have superior performance over traditional methods. Thus, it is natural to consider why deep-learning-based denoising methods are better.

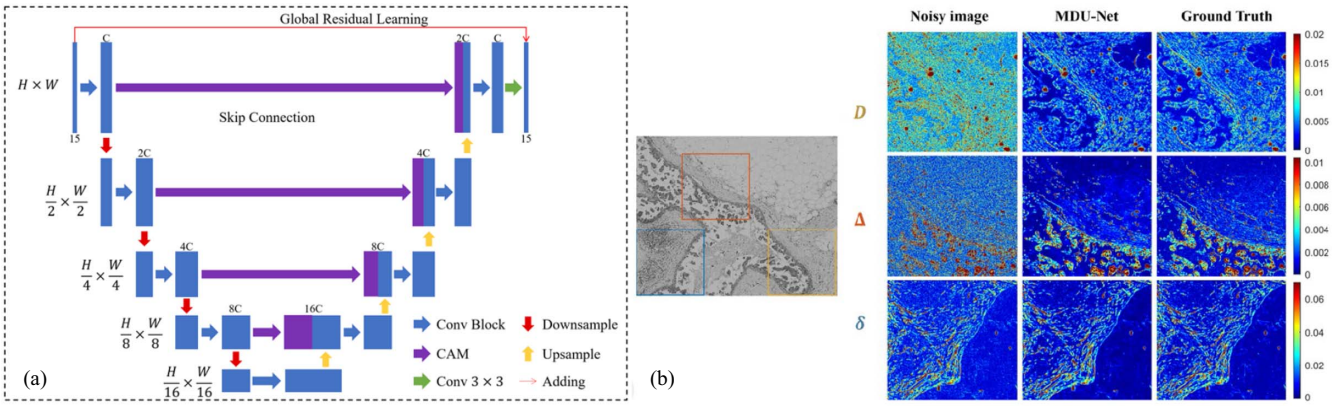

Fig. 18 Deep learning for denoising in Mueller matrix images[41]. (a) Network structure; (b) the denoised images. D: diattenuation, Δ: depolarization, δ: linear retardance.

Table 9 Quantitative Denoised Results of MDU-Net.

	Mueller matrix images			$D/\Delta/\delta$		
Method	MRMSE ($\times10^{-3}$)	MPSNR (dB)	MSSIM	RMSE ($\times10^{-3}$)	PSNR (dB)	SSIM ($\times10^{-2}$)
Noisy	6.589	30.07	0.6875	5.616/3.405/5.891	31.81/36.03/29.30	68.42/69.11/84.05
MDU-Net	2.654	38.12	0.8968	2.298/1.217/2.831	39.40/45.15/35.19	90.30/94.26/95.88

Table 10 Summary of Deep Learning Denoising Methods for Extensive Polarimetric Images.

Method	Category	Application	Highlight
PJNDMNet[45]	Supervised	LWIR polarization image	Generating training data based on the polarization measurement redundancy error
DnCNN based[40]	Supervised	Polarization 3D integral image	Reconstructing 3D DoLP images with the help of DnCNN
MDU-Net[41]	Supervised	Mueller matrix image	Polarimetry basis parameter recovery based on modified U-Net

The traditional denoising algorithm usually finds the rule from the noise image first and then designs the corresponding descriptors to extract features. This process is based on previous human knowledge. However, handcrafted descriptors are not good enough to successfully identify more complex noise features. In fact, there is a lot of implicit knowledge or descriptors that can better remove noise, but these strategies are not well-conceived by humans. Deep learning is capable of developing strategies that are not perceived by humans, which is impossible with handcrafted features based on previous human knowledge. Automatically learning features by multiple hidden layers allows a network to learn nonlinear functions that are mapping noisy input to clean output directly from data, without relying entirely on human-crafted features. This means that the great nonlinear modeling capability of CNNs makes them suitable for automatically extracting optimal descriptors for image denoising without human intervention, which may be the main reason why deep learning methods can significantly outperform traditional denoising methods.

Although deep learning techniques have obtained great success in polarization image denoising, efficiently obtaining high-quality polarization information from noisy environments remains challenging. Next, we present the potential areas of further research for polarimetric image denoising and point out several as-yet-unsolved problems.

First, for conventional denoising methods, these methods typically consider extending denoising methods for conventional images to polarization images. BM3D-inspired approaches have garnered significant attention in the realm of polarimetric image denoising, with the BM3D family showcasing commendable performance in terms of both effectiveness and efficiency. Despite the success of these methods, several limitations persist. The potential points and challenges include the following:

(1) Studying how to utilize the relationships between image pixels and the correlation between their polarization information is an important avenue for exploration.

(2) One common drawback is the reliance on optimization methods during the testing phase, which can introduce complexity and computational overhead. Additionally, manual parameter tuning is often required, making the denoising process less automated and potentially less robust across different datasets or noise conditions.

(3) Most existing methods are tailored for specific denoising tasks or noise types, limiting their applicability to broader scenarios or requiring designed models for each task.

Addressing these challenges is crucial for advancing polarimetric image denoising techniques and enhancing their practical utility. Future research efforts may focus on developing more automated and adaptive denoising algorithms, as well as exploring techniques that can generalize across diverse noise profiles and imaging conditions. Besides, another crucial research direction lies in how to apply this technology to practical applications. This includes real-time denoising processing and denoising in complex environments. By mitigating these drawbacks, we can further improve the performance and versatility of polarimetric image denoising methods.

Second, for learning-based methods, the emergence of DNNs has revolutionized image denoising, offering notable advancements over traditional methods. However, despite these strides, state-of-the-art approaches still face limitations that hinder their application in real-world scenarios. These limitations include:

(1) One significant advantage of DNN methods is their ability to leverage external information to guide the training process[147]. This flexibility allows them to potentially surpass the theoretical and practical boundaries of traditional denoising techniques. However, it is essential to recognize that DNNs, particularly end-to-end networks, often lack interpretability. This characteristic makes them become black boxes; thus, it is challenging to explain and understand their internal operations.

(2) The reliance of DNN methods on high-quality training datasets and certain prior information poses significant challenges. Particularly, in practical scenarios, the paired noisy-clean polarimetric image data may be unavailable or hard to obtain.

(3) The application of DNN methods to polarimetric images remains relatively limited, indicating a promising area for future exploration. In other words, leveraging advancements

Table 11 Summary of Some Representative Methods in Polarimetric Image Denoising.

Method	Noise type	Feature	Key word
PCA-based[34]	AWGN and realistic	Noise suppression and DoLP enhancement for polarization images	Keeping the most relevant parts of polarimetric images in the PCA domain
KSVD-based[36]	AWGN	Denoising polarization images	Obtaining the optimized representation of polarization images via dictionary learning and sparse coding
PBM3D[32]	AWGN and realistic	Reducing noise of polarimetric images and enhancing S_0, DoLP, and AoP information	Applying BM3D to a chosen polarization space with the optimal denoising transformation matrix
BM3D-DoFP[35]	AWGN	Noise suppression and DoLP enhancement for polarization images	Extension of BM3D to polarimetric images using a superpixel patch
Adaptive BM3D[37]	Speckle	Suppressing speckle noise of polarization images	BM3D with an adaptive thresholding technique based on the smoothness of a polarimetric image patch
BM3D-CPFA[33]	AWGN and realistic	Color polarization image denoising and color DoLP reconstruction	Applying BM3D according to the correlation between different polarization and color channels
PDRDN[39]	Realistic	Reducing noise of polarimetric images and recovering S_0, DoLP, and AoP information	Residual dense network designed for polarimetric image denoising
CARDN[43]	Realistic	Reducing noise of polarimetric images and recovering S_0, DoLP, and AoP information	A flexible model with a channel attention block and adaptive polarization loss
IPLNet[38]	Realistic	Color polarimetric image denoising and S_0, DoLP, and AoP restoration	A denoising network with intensity polarization, two sub-nets, and one-to-three three sub-branches
ColorPolarNet[42]	Realistic	Color polarimetric image denoising and S_0, DoLP, and AoP restoration	A two-step parallel multitask CNN with a loss function based on Stokes parameters
3DCNN-based[44]	Realistic	Denoising color polarimetric images and restoring color S_0, DoLP, and AoP information	An entirely 3D denoising network with 3D convolution and color polarization loss
ViT-based[46]	Realistic	Color polarimetric image denoising and S_0, DoLP, and AoP restoration	A vision transformer model with hybrid attention mechanisms and Stokes parameter loss
PJDNDMNet[45]	Synthetic and realistic	Reducing noise of LWIR polarization images and reconstructing infrared S_0, DoLP, and AoP information	A three-stage progressive CNN guided by mixed noise level estimation
DnCNN-based[40]	AWGN	Suppressing noise of polarimetric 3D integral images and restoring S_0, DoLP, and AoP information	A physical model trained DnCNN with passive 3D polarimetric integral imaging in low-light conditions
MDU-Net[41]	Realistic	Suppressing noise of Mueller matrix images and restoring diattenuation, depolarization, and linear retardance	A modified U-Net network incorporating channel attention and Mueller matrix loss
Pol2Pol[116]	AWGN and realistic	Reducing noise of polarimetric images and recovering S_0, DoLP, and AoP information	A self-supervised model trained only with one-shot noisy polarimetric images
TL-based[114]	Realistic	Reducing noise of polarimetric images and recovering S_0, DoLP, and AoP information	Small-scale polarimetric dataset trained network by fine-tuning a pre-trained color image denoising model

in denoising networks and embracing the innovation of novel network architectures will enhance the performance and applicability of learning-based denoising methods.

Efforts to address these limitations involve developing techniques to enhance the interpretability of DNNs, such as incorporating attention mechanisms or designing architectures based on the physical information. By improving the interpretability of DNN-based denoising methods, researchers aim to enhance their trustworthiness and facilitate their adoption in piratical real-world applications. Thus, developing physically informed models, which integrate polarization information with the learning-based method, is an important direction. To mitigate the limitation of the dataset, self-supervised learning approaches integrated into CNNs offer promise for real noisy image

denoising or blind denoising tasks. Additionally, TL and GANs represent alternative learning-based methods that address the critical issue of insufficient training data[148]. Expanding the repertoire of CNN-based methods for denoising polarimetric images could yield substantial benefits.

In addition to using polarization information alone, using multi-sensor fusion methods[149] can further improve image enhancement, such as the fusion of infrared images and color images. Enhancing imaging hardware components to effectively suppress noise is a potential solution for capturing high-quality images. Additionally, addressing issues like blurriness, low resolution, and corruption in a polarimetric image has certain engineering value. Hence, a recent trend focuses on simultaneously addressing image denoising along with other computer vision degradation tasks such as dehazing[150,151] and demoisacking[44]. The primary development objectives of polarization image denoising technology involve maximizing the preservation of polarization information, refining the implementation of denoising techniques, and minimizing noise interference in optical imaging.

7. Conclusion

Noise is an obstacle to high-quality polarization imaging and its practical application in polarization imaging. Therefore, denoising is a key problem in polarization imaging research. In this paper, we conduct a comprehensive survey of various techniques for denoising polarimetric images. We present a detailed analysis of representative denoising methods for polarimetric images, highlighting their characteristics and key features. Our aim is to provide readers with a clear understanding of the different concepts and methodologies that have emerged in recent years. Furthermore, we identify potential points for further research and discuss the challenges that remain in the field of polarimetric image denoising. We hope to contribute to the ongoing development of polarimetric image denoising techniques.

In summary, polarization image denoising technology is still in its early stages, and different types of denoising methods still have room for further development. From the available literature, it is evident that CNNs exhibit significant potential in removing noise from polarimetric images. However, in the real world, noise is complex and irregular. Incorporating physical and polarization information to enhance interpretability and denoising performance is very important. Furthermore, obtaining noise-free polarization images can be very challenging in practical applications. Therefore, it is critical to fully explore and utilize new learning approaches, such as unsupervised learning and self-supervised learning. Moreover, existing denoising methods have not fully benefited from the rapid development of deep learning. The application of advanced models holds promise to further enhance the denoising efficiency of polarization images. These are urgent challenges that researchers and scholars need to address.

Acknowledgments

This work was supported by the National Key Research and Development Program of China (No. 2023YFC3108500) and the National Natural Science Foundation of China (Nos. 62075161 and 62205243). The authors declare that they have no known competing financial interests or personal relationships that could have appeared to influence the work reported in this paper.

References

1. T. Tirer and R. Giryes, "Back-projection based fidelity term for ill-posed linear inverse problems," *IEEE Trans. Image Process.* **29**, 6164 (2020).
2. S. Minaee *et al.*, "Deep learning-based text classification: a comprehensive review," *ACM Comput. Surv.* **54**, 1 (2021).
3. Z.-Q. Zhao *et al.*, "Object detection with deep learning: a review," *IEEE Trans. Neural Networks Learn. Syst.* **30**, 3212 (2019).
4. S. Minaee *et al.*, "Image segmentation using deep learning: a survey," *IEEE Trans. Pattern Anal. Mach. Intell.* **44**, 3523 (2021).
5. S. P. Morgan and I. M. Stockford, "Surface-reflection elimination in polarization imaging of superficial tissue," *Opt. Lett.* **28**, 114 (2003).
6 M. E. Paoletti *et al.*, "Deep learning classifiers for hyperspectral imaging: a review," *ISPRS J. Photogramm. Remote Sens.* **158**, 279 (2019).
7. L. Schermelleh *et al.*, "Super-resolution microscopy demystified," *Nat. Cell Biol.* **21**, 72 (2019).
8. M. Boffety, H. Hu, and F. Goudail, "Contrast optimization in broadband passive polarimetric imaging," *Opt. Lett.* **39**, 6759 (2014).
9. S. Tominaga and A. Kimachi, "Polarization imaging for material classification," *Opt. Eng.* **47**, 123201 (2008).
10. X. Fan *et al.*, "TSMPN-PSI: high-performance polarization scattering imaging based on three-stage multi-pipeline networks," *Opt. Express* **31**, 38097 (2023).
11. X. Li *et al.*, "Polarimetric imaging through scattering media: a review," *Front. Phys.* **10**, 815296 (2022).
12. Y. Xiang *et al.*, "Underwater polarization imaging recovery based on polarimetric residual dense network," *IEEE Photonics J.* **14**, 7860206 (2022).
13. F. Drouet *et al.*, "3D reconstruction of external and internal surfaces of transparent objects from polarization state of highlights," *Opt. Lett.* **39**, 2955 (2014).
14. X. Li *et al.*, "Near-infrared monocular 3D computational polarization imaging of surfaces exhibiting nonuniform reflectance," *Opt. Express* **29**, 15616 (2021).
15. S. Li *et al.*, "Development status and key technologies of polarization imaging detection," *Chin. J. Opt.* **6**, 803 (2013).
16. X. Fan, B. Lin, and Z. Guo, "Infrared polarization-empowered full-time road detection via lightweight multi-pathway collaborative 2D/3D convolutional networks," *IEEE Trans. Intell. Transp. Syst.* (2024), p. 12762.
17. Z. Guan *et al.*, "Contrast optimization in broadband passive polarimetric imaging based on color camera," *Opt. Express* **27**, 2444 (2019).
18. N. Ghosh and I. A. Vitkin, "Tissue polarimetry: concepts, challenges, applications, and outlook," *J. Biomed Opt.* **16**, 110801 (2011).
19. J. Hao *et al.*, "A micro-polarizer array configuration design method for division of focal plane imaging polarimeter," *IEEE Sens. J.* **21**, 2828 (2020).
20. J. Bai *et al.*, "Chip-integrated plasmonic flat optics for mid-infrared full-stokes polarization detection," *Photonics Res.* **7**, 1051 (2019).
21. S. Gao and V. Gruev, "Bilinear and bicubic interpolation methods for division of focal plane polarimeters," *Opt. Express* **19**, 26161 (2011).
22. X. Shen, A. Carnicer, and B. Javidi, "Three-dimensional polarimetric integral imaging under low illumination conditions," *Opt. Lett.* **44**, 3230 (2019).
23. J. Liang and L. V. Wang, "Single-shot ultrafast optical imaging," *Optica* **5**, 1113 (2018).
24. S. Liu *et al.*, "A new polarization image demosaicking algorithm by exploiting inter-channel correlations with guided filtering," *IEEE Trans. Image Process.* **29**, 7076 (2020).

25. R. Wu *et al.*, "Polarization image demosaicking using polarization channel difference prior," *Opt. Express* **29**, 22066 (2021).
26. B. Lin *et al.*, "Dynamic polarization fusion network (DPFN) for imaging in different scattering systems," *Opt. Express* **32**, 511 (2024).
27. K. Usmani *et al.*, "Three-dimensional polarimetric integral imaging in photon-starved conditions: performance comparison between visible and long wave infrared imaging," *Opt. Express* **28**, 19281 (2020).
28. R. Chen *et al.*, "Image-denoising algorithm based on improved K-singular value decomposition and atom optimization," *CAAI Trans. Intell. Technol.* **7**, 117 (2022).
29. Y.-C. Heo, K. Kim, and Y. Lee, "Image denoising using nonlocal means (NLM) approach in magnetic resonance (MR) imaging: a systematic review," *Appl. Sci.* **10**, 7028 (2020).
30. K. Dabov *et al.*, "Image denoising by sparse 3-D transform-domain collaborative filtering," *IEEE Trans. Image Process.* **16**, 2080 (2007).
31. A. Abubakar *et al.*, "A hybrid denoising algorithm of BM3D and KSVD for Gaussian noise in DoFP polarization images," *IEEE Access* **8**, 57451 (2020).
32. A. B. Tibbs *et al.*, "Denoising imaging polarimetry by adapted BM3D method," *J. Opt. Soc. Am. A* **35**, 690 (2018).
33. J.-A. Liang, Y.-F. Guo, and B. Liu, "BM3D-based denoising method for color polarization filter array," *Opt. Express* **30**, 22107 (2022).
34. J. Zhang *et al.*, "PCA-based denoising method for division of focal plane polarimeters," *Opt. Express* **25**, 2391 (2017).
35. A. Abubakar *et al.*, "A block-matching and 3-D filtering algorithm for gaussian noise in DoFP polarization images," *IEEE Sens. J.* **18**, 7429 (2018).
36. W. Ye *et al.*, "AK times singular value decomposition based image denoising algorithm for DoFP polarization image sensors with Gaussian noise," *IEEE Sens. J.* **18**, 6138 (2018).
37. A. Abubakar and A. Bermak, "An adaptive denoising algorithm for speckle noise in DoFP polarization images," in *4th International Conference on Circuits, Systems and Simulation (ICCSS)* (2021), p. 225.
38. H. Hu *et al.*, "IPLNet: a neural network for intensity-polarization imaging in low light," *Opt. Lett.* **45**, 6162 (2020).
39. X. Li *et al.*, "Learning-based denoising for polarimetric images," *Opt. Express* **28**, 16309 (2020).
40. K. Usmani, T. O'Connor, and B. Javidi, "Three-dimensional polarimetric image restoration in low light with deep residual learning and integral imaging," *Opt. Express* **29**, 29505 (2021).
41. X. Yang *et al.*, "Deep learning for denoising in a Mueller matrix microscope," *Biomed Opt. Express* **13**, 3535 (2022).
42. X. Xu *et al.*, "ColorPolarNet: residual dense network-based chromatic intensity-polarization imaging in low-light environment," *IEEE Trans. Instrum. Meas.* **71**, 5025210 (2022).
43. H. Liu *et al.*, "Attention-based neural network for polarimetric image denoising," *Opt. Lett.* **47**, 2726 (2022).
44. J. Liu *et al.*, "Polarization image demosaicing and RGB image enhancement for a color polarization sparse focal plane array," *Opt. Express* **31**, 23475 (2023).
45. N. Li *et al.*, "Joint denoising-demosaicking network for long-wave infrared division-of-focal-plane polarization images with mixed noise level estimation," *IEEE Trans. Image Process.* (2023), p. 5961.
46. Z. Li *et al.*, "Polarized color image denoising," in *IEEE/CVF Conference on Computer Vision and Pattern Recognition (CVPR)* (2023), p. 9873.
47. A. E. Ilesanmi and T. O. Ilesanmi, "Methods for image denoising using convolutional neural network: a review," *Complex Intell. Syst.* **7**, 2179 (2021).
48. M. Tripathi, "Facial image denoising using AutoEncoder and UNET," *Herit. Sustain. Dev.* **3**, 89 (2021).
49. W. Jifara *et al.*, "Medical image denoising using convolutional neural network: a residual learning approach," *J. Supercomput.* **75**, 704 (2019).
50. C. Tian, Y. Xu, and W. Zuo, "Image denoising using deep CNN with batch renormalization," *Neural Netw.* **121**, 461 (2020).
51. V. Deschaintre, Y. Lin, and A. Ghosh, "Deep polarization imaging for 3D shape and SVBRDF acquisition," in *Proceedings of the IEEE/CVF Conference on Computer Vision and Pattern Recognition* (2021), p. 15567.
52. Y. Sun, J. Zhang, and R. Liang, "Color polarization demosaicking by a convolutional neural network," *Opt. Lett.* **46**, 4338 (2021).
53. J. Weng, C. Gao, and B. Lei, "Real-time polarization measurement based on spatially modulated polarimeter and deep learning," *Results Phys.* **46**, 106280 (2023).
54. P. Qi *et al.*, "U2R-pGAN: unpaired underwater-image recovery with polarimetric generative adversarial network," *Opt. Lasers Eng.* **157**, 107112 (2022).
55. Z. Chen *et al.*, "DN-GAN: denoising generative adversarial networks for speckle noise reduction in optical coherence tomography images," *Biomed. Signal Process. Control* **55**, 101632 (2020).
56. H. Wang *et al.*, "Joint noise reduction for contrast enhancement in stokes polarimetric imaging," *IEEE Photonics J.* **11**, 6901010 (2019).
57. S. Qiu *et al.*, "Linear polarization demosaicking for monochrome and colour polarization focal plane arrays," in *Computer Graphics Forum*, Vol. **40** (Wiley Online Library, 2021), p. 77.
58. D. H. Goldstein, *Polarized Light* (CRC Press, 2017).
59. K. Wei *et al.*, "A physics-based noise formation model for extreme low-light raw denoising," in *Proceedings of the IEEE/CVF Conference on Computer Vision and Pattern Recognition* (2020), p. 2758.
60. K. Wei *et al.*, "Physics-based noise modeling for extreme low-light photography," *IEEE Trans. Pattern Anal. Mach. Intell.* **44**, 8520 (2021).
61. R. L. Baer, "A model for dark current characterization and simulation," in *Sensors, Cameras, and Systems for Scientific/Industrial Applications VII*, Vol. **6068** (SPIE, 2006), p. 37.
62. A. K. Boyat and B. K. Joshi, "A review paper: noise models in digital image processing," arXiv:1505.03489 (2015).
63. X. Li *et al.*, "Optimal distribution of integration time for intensity measurements in Stokes polarimetry," *Opt. Express* **23**, 27690 (2015).
64. C. Zhou *et al.*, "Polarization-aware low-light image enhancement," in *Proceedings of the AAAI Conference on Artificial Intelligence* (2023), p. 3742.
65. B. Goyal *et al.*, "Image denoising review: from classical to state-of-the-art approaches," *Inf. Fusion* **55**, 220 (2020).
66. T. F. Chan, S. Osher, and J. Shen, "The digital TV filter and nonlinear denoising," *IEEE Trans. Image Process.* **10**, 231 (2001).
67. S. Lefkimmiatis, "Non-local color image denoising with convolutional neural networks," in *Proceedings of the IEEE Conference on Computer Vision and Pattern Recognition* (2017), p. 3587.
68. J. V. Manjón *et al.*, "MRI denoising using non-local means," *Med. Image Anal.* **12**, 514 (2008).
69. A. Buades, B. Coll, and J.-M. Morel, "A non-local algorithm for image denoising," in *IEEE Computer Society Conference on Computer Vision and Pattern Recognition (CVPR'05)* (2005), p. 60.
70. L. P. Yaroslavsky, K. O. Egiazarian, and J. T. Astola, "Transform domain image restoration methods: review, comparison, and interpretation," *Proc. SPIE* **4304**, 155 (2001).
71. J. Portilla *et al.*, "Image denoising using scale mixtures of Gaussians in the wavelet domain," *IEEE Trans. Image Process.* **12**, 1338 (2003).

72. L. Zhang *et al.*, "PCA-based spatially adaptive denoising of CFA images for single-sensor digital cameras," *IEEE Trans. Image Process.* **18**, 797 (2009).
73. L. Zhang *et al.*, "Two-stage image denoising by principal component analysis with local pixel grouping," *Pattern Recognit.* **43**, 1531 (2010).
74. K. Dabov *et al.*, "BM3D image denoising with shape-adaptive principal component analysis," in *SPARS'09-Signal Processing with Adaptive Sparse Structured Representations* (2009).
75. M. Elad and M. Aharon, "Image denoising via sparse and redundant representations over learned dictionaries," *IEEE Trans. Image Process.* **15**, 3736 (2006).
76. Q. Guo *et al.*, "An efficient SVD-based method for image denoising," *IEEE Trans. Circuits Syst. Video Technol.* **26**, 868 (2015).
77. K. Zhang, W. Zuo, and L. Zhang, "FFDNet: toward a fast and flexible solution for CNN-based image denoising," *IEEE Trans. Image Process.* **27**, 4608 (2018).
78. K. Zhang *et al.*, "Beyond a Gaussian denoiser: residual learning of deep CNN for image denoising," *IEEE Trans. Image Process.* **26**, 3142 (2017).
79. C. Tian *et al.*, "A cross transformer for image denoising," *Inf. Fusion* **102**, 102043 (2024).
80. Y. Zhao *et al.*, "Low-frequency noise suppression method based on improved DnCNN in desert seismic data," *IEEE Geosci. Remote Sens. Lett.* **16**, 811 (2018).
81. S. Ioffe and C. Szegedy, "Batch normalization: accelerating deep network training by reducing internal covariate shift," in *International Conference on Machine Learning* (2015), p. 448.
82. V. Nair and G. E. Hinton, "Rectified linear units improve restricted Boltzmann machines," in *Proceedings of the 27th International Conference on Machine Learning (ICML-10)* (2010), p. 807.
83. M. Shafiq and Z. Gu, "Deep residual learning for image recognition: a survey," *Appl. Sci.* **12**, 8972 (2022).
84. K. He *et al.*, "Deep residual learning for image recognition," in *Proceedings of the IEEE Conference on Computer Vision and Pattern Recognition* (2016), p. 770.
85. G. Huang *et al.*, "Densely connected convolutional networks," in *Proceedings of the IEEE Conference on Computer Vision and Pattern Recognition* (2017), p. 4700.
86. Y. Zhang *et al.*, "Residual dense network for image super-resolution," in *Proceedings of the IEEE Conference on Computer Vision and Pattern Recognition* (2018), p. 2472.
87. Y. Zhang *et al.*, "Residual dense network for image restoration," *IEEE Trans. Pattern Anal. Mach. Intell.* **43**, 2480 (2020).
88. B. Park, S. Yu, and J. Jeong, "Densely connected hierarchical network for image denoising," in *IEEE/CVF Conference on Computer Vision and Pattern Recognition Workshops (CVPRW)* (2019), p. 2104.
89. Q. Zhang *et al.*, "A parallel and serial denoising network," *Expert Syst. Appl.* **231**, 120628 (2023).
90. C. Tian *et al.*, "Multi-stage image denoising with the wavelet transform," *Pattern Recognit.* **134**, 109050 (2023).
91. C. Tian *et al.*, "Heterogeneous window transformer for image denoising," arXiv:2407.05709 (2024).
92. J. Lehtinen *et al.*, "Noise2noise: learning image restoration without clean data," in *Proceedings of the 35th International Conference on Machine Learning* (2018), p. 2965.
93. C. Tian *et al.*, "A self-supervised network for image denoising and watermark removal," *Neural Netw.* **174**, 106218 (2024).
94. C. Tian *et al.*, "Perceptive self-supervised learning network for noisy image watermark removal," *IEEE Trans. Circuits Syst. Video Technol.* **34**, 7069 (2024).
95. B. Ding *et al.*, "U^2D^2Net: unsupervised unified image dehazing and denoising network for single hazy image enhancement," *IEEE Trans. Multimedia* **26**, 202 (2024).
96. M. Aharon, M. Elad, and A. Bruckstein, "K-SVD: an algorithm for designing overcomplete dictionaries for sparse representation," *IEEE Trans. Signal Process.* **54**, 4311 (2006).
97. B. Dumitrescu and P. Irofti, "Regularized K-SVD," *IEEE Signal Process Lett.* **24**, 309 (2017).
98. T. T. Cai and L. Wang, "Orthogonal matching pursuit for sparse signal recovery with noise," *IEEE Trans. Inf. Theory* **57**, 4680 (2011).
99. J. Wang, S. Kwon, and B. Shim, "Generalized orthogonal matching pursuit," *IEEE Trans. Signal Process.* **60**, 6202 (2012).
100. K. Dabov *et al.*, "Color image denoising via sparse 3D collaborative filtering with grouping constraint in luminance-chrominance space," in *IEEE International Conference on Image Processing* (2007).
101. Y. LeCun, Y. Bengio, and G. Hinton, "Deep learning," *Nature* **521**, 436 (2015).
102. J. Redmon *et al.*, "You only look once: unified, real-time object detection," in *Proceedings of the IEEE Conference on Computer Vision and Pattern Recognition* (2016), p. 779.
103. Y.-J. Cha, W. Choi, and O. Büyüköztürk, "Deep learning-based crack damage detection using convolutional neural networks," *Comput. Aided Civ. Infrastruct. Eng.* **32**, 361 (2017).
104. K. Zhang *et al.*, "Learning deep CNN denoiser prior for image restoration," in *Proceedings of the IEEE Conference on Computer Vision and Pattern Recognition* (2017), p. 3929.
105. Q. Yuan *et al.*, "Deep learning in environmental remote sensing: achievements and challenges," *Remote Sens. Environ.* **241**, 111716 (2020).
106. Y. Ba *et al.*, "Deep shape from polarization," in *Computer Vision–ECCV 2020: 16th European Conference* (Springer, 2020), p. 554.
107. C. Zhou *et al.*, "Learning to dehaze with polarization," in *Advances in Neural Information Processing Systems*, Vol. **34** (2021), p. 11487.
108. D. Li *et al.*, "High-performance polarization remote sensing with the modified u-net based deep-learning network," *IEEE Trans. Geosci. Remote Sens.* **60**, 1 (2022).
109. J. Hu, L. Shen, and G. Sun, "Squeeze-and-excitation networks," in *Proceedings of the IEEE Conference on Computer Vision and Pattern Recognition* (2018), p. 7132.
110. Y. Kim *et al.*, "Transfer learning from synthetic to real-noise denoising with adaptive instance normalization," in *Proceedings of the IEEE/CVF Conference on Computer Vision and Pattern Recognition* (2020), p. 3482.
111. C. Tan *et al.*, "A survey on deep transfer learning," in *Artificial Neural Networks and Machine Learning–ICANN 2018: 27th International Conference on Artificial Neural Networks* (Springer, 2018), p. 270.
112. K. Sohn *et al.*, "Unsupervised domain adaptation for face recognition in unlabeled videos," in *Proceedings of the IEEE International Conference on Computer Vision* (2017), p. 3210.
113. M. Long *et al.*, "Deep transfer learning with joint adaptation networks," in *International Conference on Machine Learning* (2017), p. 2208.
114. H. Hu *et al.*, "Polarimetric image denoising on small datasets using deep transfer learning," *Opt. Laser Technol.* **166**, 109632 (2023).
115. T. Plotz and S. Roth, "Benchmarking denoising algorithms with real photographs," in *Proceedings of the IEEE Conference on Computer Vision and Pattern Recognition* (2017), p. 1586.
116. H. Liu *et al.*, "Pol2Pol: self-supervised polarimetric image denoising," *Opt. Lett.* **48**, 4821 (2023).
117. N. Moran *et al.*, "Noisier2noise: Learning to denoise from unpaired noisy data," in *IEEE/CVF Conference on Computer Vision and Pattern Recognition (CVPR)* (2020), p. 12061.
118. A. Krull, T. O. Buchholz, and F. Jug, "Noise2Void-learning denoising from single noisy images," in *IEEE/CVF Conference*

on Computer Vision and Pattern Recognition (CVPR) (2019), p. 2129.
119. Z. Wang *et al.*, "Blind2unblind: self-supervised image denoising with visible blind spots," in *IEEE/CVF Conference on Computer Vision and Pattern Recognition (CVPR)* (2022), p. 2017.
120. T. Huang *et al.*, "Neighbor2neighbor: a self-supervised framework for deep image denoising," *IEEE Trans. Image Process.* **31**, 4023 (2022).
121. M. Morimatsu *et al.*, "Monochrome and color polarization demosaicking based on intensity-guided residual interpolation," *IEEE Sens. J.* **21**, 26985 (2021).
122. S. Qiu *et al.*, "Polarization demosaicking for monochrome and color polarization focal plane arrays," in *International Symposium on Vision, Modeling and Visualization* (The Eurographics Association, 2019).
123. C. Tian *et al.*, "Deep learning on image denoising: an overview," *Neural Netw.* **131**, 251 (2020).
124. X. Ying *et al.*, "Deformable 3D convolution for video super-resolution," *IEEE Signal Process Lett.* **27**, 1500 (2020).
125. A. Vaswani *et al.*, "Attention is all you need," in *NIPS'17: Proceedings of the 31st International Conference on Neural Information Processing Systems* (2017).
126. K. Han *et al.*, "A survey on vision transformer," *IEEE Trans. Pattern Anal. Mach. Intell.* **45**, 87 (2022).
127. B. Lin, X. Fan, and Z. Guo, "Self-attention module in a multi-scale improved U-net (SAM-MIU-net) motivating high-performance polarization scattering imaging," *Opt. Express* **31**, 3046 (2023).
128. Z. Wang *et al.*, "Uformer: a general u-shaped transformer for image restoration," in *Proceedings of the IEEE/CVF Conference on Computer Vision and Pattern Recognition* (2022), p. 17683.
129. S. W. Zamir *et al.*, "Restormer: efficient transformer for high-resolution image restoration," in *Proceedings of the IEEE/CVF Conference on Computer Vision and Pattern Recognition* (2022), p. 5728.
130. S. Komatsu *et al.*, "Three-dimensional integral imaging and object detection using long-wave infrared imaging," *Appl. Opt.* **56**, D120 (2017).
131. P. Wani *et al.*, "Lowlight object recognition by deep learning with passive three-dimensional integral imaging in visible and long wave infrared wavelengths," *Opt. Express* **30**, 1205 (2022).
132. D. B. Chenault *et al.*, "Metrics for comparison of polarimetric and thermal target to background contrast," in *IEEE Research and Applications of Photonics in Defense Conference (RAPID)* (2018).
133. J. L. Pezzaniti *et al.*, "Detection of obscured targets with IR polarimetric imaging," in *Detection and Sensing of Mines, Explosive Objects, and Obscured Targets XIX* (2014), p. 347.
134. N. Li *et al.*, "Removal of reflections in LWIR image with polarization characteristics," *Opt. Express* **26**, 16488 (2018).
135. N. Li *et al.*, "Joint denoising-demosaicking network for long-wave infrared division-of-focal-plane polarization images with mixed noise level estimation," *IEEE Trans. Image Process.* **32**, 5961 (2023).
136. N. Li *et al.*, "No-reference physics-based quality assessment of polarization images and its application to demosaicking," *IEEE Trans. Image Process.* **30**, 8983 (2021).
137. B. L. Teurnier *et al.*, "Definition of an error map for DoFP polarimetric images and its application to retardance calibration," *Opt. Express* **30**, 9534 (2022).
138. B. Tavakoli, B. Javidi, and E. Watson, "Three dimensional visualization by photon counting computational integral imaging," *Opt. Express* **16**, 4426 (2008).
139. A. Markman, X. Shen, and B. Javidi, "Three-dimensional object visualization and detection in low light illumination using integral imaging," *Opt. Lett.* **42**, 3068 (2017).
140. A. Stern, D. Aloni, and B. Javidi, "Experiments with three-dimensional integral imaging under low light levels," *IEEE Photonics J.* **4**, 1188 (2012).
141. V. V. Tuchin, "Polarized light interaction with tissues," *J. Biomed Opt.* **21**, 071114 (2016).
142. J. Zhou *et al.*, "Modulus design multiwavelength polarization microscope for transmission Mueller matrix imaging," *J. Biomed Opt.* **23**, 016007 (2018).
143. G. Anna and F. Goudail, "Optimal Mueller matrix estimation in the presence of Poisson shot noise," *Opt. Express* **20**, 21331 (2012).
144. O. Ronneberger, P. Fischer, and T. Brox, "U-net: convolutional networks for biomedical image segmentation," in *Medical Image Computing and Computer-Assisted Intervention–MICCAI 2015: 18th International Conference* (Springer, 2015), p. 234.
145. D. Li *et al.*, "High-performance polarization remote sensing with the modified U-net based deep-learning network," *IEEE Trans. Geosci. Remote Sens.* **60**, 5621110 (2022).
146. S. Woo *et al.*, "CBAM: convolutional block attention module," in *Proceedings of the European Conference on Computer Vision (ECCV)* (2018), p. 3.
147. X. Fan *et al.*, "Improved polarization scattering imaging using local-global context polarization feature learning framework," *Opt. Lasers Eng.* **178**, 108194 (2024).
148. H. Zhou *et al.*, "Polarization motivating high-performance weak targets' imaging based on a dual-discriminator GAN," *Opt. Express* **32**, 3835 (2024).
149. A. Zhong *et al.*, "Performance analysis of joint imaging system with polarized, infrared, and visible cameras for multi-sensor imaging," *Optik* **295**, 171512 (2023).
150. Y. Wei *et al.*, "Polarization descattering imaging: a solution for nonuniform polarization characteristics of a target surface," *Chin. Opt. Lett.* **19**, 111101 (2021).
151. X. Fan *et al.*, "TSMPN-PSI: high-performance polarization scattering imaging based on three-stage multi-pipeline networks," *Opt. Express* **31**, 38097 (2023).